International Journal of Extreme Manufacturing

TOPICAL REVIEW • OPEN ACCESS

A review of the fabrication of twisted two-dimensional material moiré structures

To cite this article: Jichuang Shen *et al* 2026 *Int. J. Extrem. Manuf.* **8** 032007

OPEN ACCESS
IMMT | IOP Publishing
International Journal of Extreme Manufacturing
Int. J. Extrem. Manuf. **8** (2026) 032007 (26pp)
https://doi.org/10.1088/2631-7990/ae35e9

Topical Review

A review of the fabrication of twisted two-dimensional material moiré structures

Jichuang Shen[1,2], Han Chen[1,2], Wenhao Li[1,2], Chen Ji[1,2], Huaze Zhu[2,*] and Wei Kong[2,3,4,*]

[1] School of Materials Science and Engineering, Zhejiang University, Hangzhou 310027, People's Republic of China
[2] Key Laboratory of 3D Micro/Nano Fabrication and Characterization of Zhejiang Province, School of Engineering, Westlake University, Hangzhou 310030, People's Republic of China
[3] Research Center for Industries of the Future, Westlake University, Hangzhou, 310030 Zhejiang, People's Republic of China
[4] Zhejiang Key Laboratory of 3D Micro/Nano Fabrication and Characterization, Westlake Institute for Optoelectronics, Fuyang, Hangzhou, Zhejiang 311400, People's Republic of China

E-mail: zhuhuaze@westlake.edu.cn and kongwei@westlake.edu.cn

Received 17 August 2024, revised 2 September 2025
Accepted for publication 8 January 2026
Published 3 February 2026

Abstract

Stacking two layers of two-dimensional (2D) materials at a twisted angle produces the Moiré structure, which can give rise to novel quantum-correlated states. The topology, periodicity, and direction of the resulting Moiré superlattice are strongly influenced by the twist angle, making it crucial to prepare stacked 2D structures with controllable angles to precisely regulate the properties of 2D materials. This review outlines the topological design principles of Moiré patterns, investigates the impact of twist angles on their morphology and periodicity, and summarizes the diverse properties exhibited by 2D systems at different twist angles. The fabrication methods for twisted 2D structures, such as direct growth and artificial manipulation, are analyzed alongside strategies for accurate twist angle control. Additionally, this review highlights state-of-the-art ultraclean transfer in vacuum, in-situ dynamic twisting technologies and the development of novel multilayer twisted 2D structures. Finally, the remaining challenges in the fabrication of twisted 2D Moiré structures are discussed, along with potential solutions to address these challenges.

Keywords: twist-angle 2D materials, moiré superlattices, moiré fabrication

* Authors to whom any correspondence should be addressed.

Introduction

Since the artificial exfoliation of monolayer graphene (Gr) in 2004[1], this single-layer two-dimensional (2D) carbon material has exhibited strikingly different physical and chemical properties compared to its bulk material, such as ultra-high electron mobility[2,3], exceptional thermal conductivity[4], and remarkable mechanical properties[5,6]. With over 2 000 known 2D materials[7,8], this family of 2D crystals encompasses a wide range of electronic structures: metals (graphene)[9,10], semiconductors such as black phosphorus, BP and some transition metal dichalcogenides (TMDCs)[11,12], and insulators (hexagonal boron nitride, h-BN)[13,14]. These materials offer significant potential for research and applications in various fields, including electronics, optoelectronics, and thermal management[15–18].

Furthermore, by stacking two layers of 2D materials with a specific twist angle, a Moiré superlattice with defined periodicity is formed[19–22]. As the twist angle changes, the periodicity of the Moiré pattern within this superlattice also shifts, altering the interlayer interactions and modifying the electronic states and physical properties. For example, twisted bilayer graphene (*t*-BLG) at an angle around 1.1° exhibits Mott insulating behavior and unconventional superconductivity due to the emergence of flat bands within the Moiré superlattice[23]. Recent studies have also revealed unique properties of *t*-BLG beyond the "magic angle" range[19,24], as well as novel phenomena such as Moiré excitons in twisted 2D materials beyond graphene[21,25]. These findings highlight the crucial role of twisting in modulating the properties of stacked 2D systems. Consequently, the precise fabrication of twisted 2D structures is not only a promising approach for creating new 2D quantum platforms but also a key technology for controlling their properties.

There are two primary strategies for constructing twisted 2D superlattices: direct growth and artificial manipulation. Figure 1 summarizes the historical advancements in twisted 2D superlattice fabrication over the past four decades. As shown in Figure 1(a), Moiré patterns with varying periodicities were first observed on highly oriented pyrolytic graphite (HOPG) using scanning tunneling microscopy (STM) in 1988, which was attributed to the rotational stacking of surface graphene[26]. Around 2010, twisted graphene was successfully grown on SiC and Cu substrates, facilitated by advancements in epitaxial growth and chemical vapor deposition (CVD) techniques[27–30]. After 2021, researchers achieved the growth of *t*-BLG over the full range of twist angles (0°–30°) and twisted bilayer MoS_2 (*t*-MoS_2) across a 0°–60° range[31–34]. Recent CVD innovations have further enabled precise control of the twist angle in *t*-BLG growth[35].

In addition to direct growth, artificial manipulation methods, illustrated in Figure 1(b), have been extensively developed to fabricate twisted 2D materials. Techniques such as flipped folding, rotational pushing, and twisted stacking are commonly employed. Theoretically, folding a monolayer 2D material at a specific angle can create a twisted bilayer structure. As early as 1993, graphene folding was observed on HOPG surfaces via STM[36,49]. Inspired by this, researchers later developed STM and (AFM) tip-assisted graphene folding techniques[37,50–52]. Following the successful isolation of monolayer graphene in 2004, water flushing became the simplest method for producing folded graphene[38,53,54]. Over the past two decades, advancements in 2D material transfer technologies have enabled the construction of large-area, full-range twisted structures such as *t*-BLG and *t*-MoS_2 through transfer and twisted assembly techniques[39–41]. Modern transfer and stacking methods ensure clean interfaces under vacuum conditions[46,47,55], allow for continuous multi-layer twisted stacking[42,56,57], and enable dynamic control of the twist angle[43–45,48,58].

Although many previous reviews have focused on the stacking engineering of twisted bilayer systems[59,60], and have discussed the rich properties of 2D Moiré materials[21,25,61–63], comprehensive discussions on the theoretical design, construction methods, and impact on the properties of Moiré structures are scarce. Other reviews summarize various methods for creating 2D twisted structures[24,64–66] but often overlook the precision required in controlling the stacking angles. Therefore, this review aims to provide a timely and systematic overview of the basic principles, properties, and fabrication methods of twisted 2D materials. In the first section, we discussed the relationship among 2D Moiré morphology, periodicity, and twist angle, along with the influence of twisting on the material properties. In the second section, we review the methods for obtaining twisted Moiré structures through direct growth and artificial manipulations. For the direct growth method, we discussed the key issues in the growth of twisted homojunctions, heterojunctions, and spiral superlattices of graphene, h-BN, TMDC, and other 2D materials. For artificial manipulations, two principal techniques are employed: macro-scale twisted stacking and micro-scale in-situ manipulation, with a particular focus on precise control of the twist angle. Finally, we present an outlook on the current challenges and future directions in the research on 2D twisted Moiré materials.

1. 2D Moiré design

Under specific twist angles and lattice mismatches in Moiré superlattices, a new electronic state is introduced to the 2D stacked system. For example, the flat-band associated state emerges in bilayer graphene at a small twist angle[67,68]. Moiré potential[69,70] and interlayer excitons have also been discovered in twisted TMDCs systems[70–72]. The properties of these novel electronic states in 2D systems are intricately linked to the material categories, Moiré periodicity, and geometric morphology.

1.1. Moiré pattern topology

The topological morphology of Moiré superlattices is closely related to the crystal system of the primitive 2D materials. Graphene, h-BN, TMDCs, and bismuthene crystallize in a

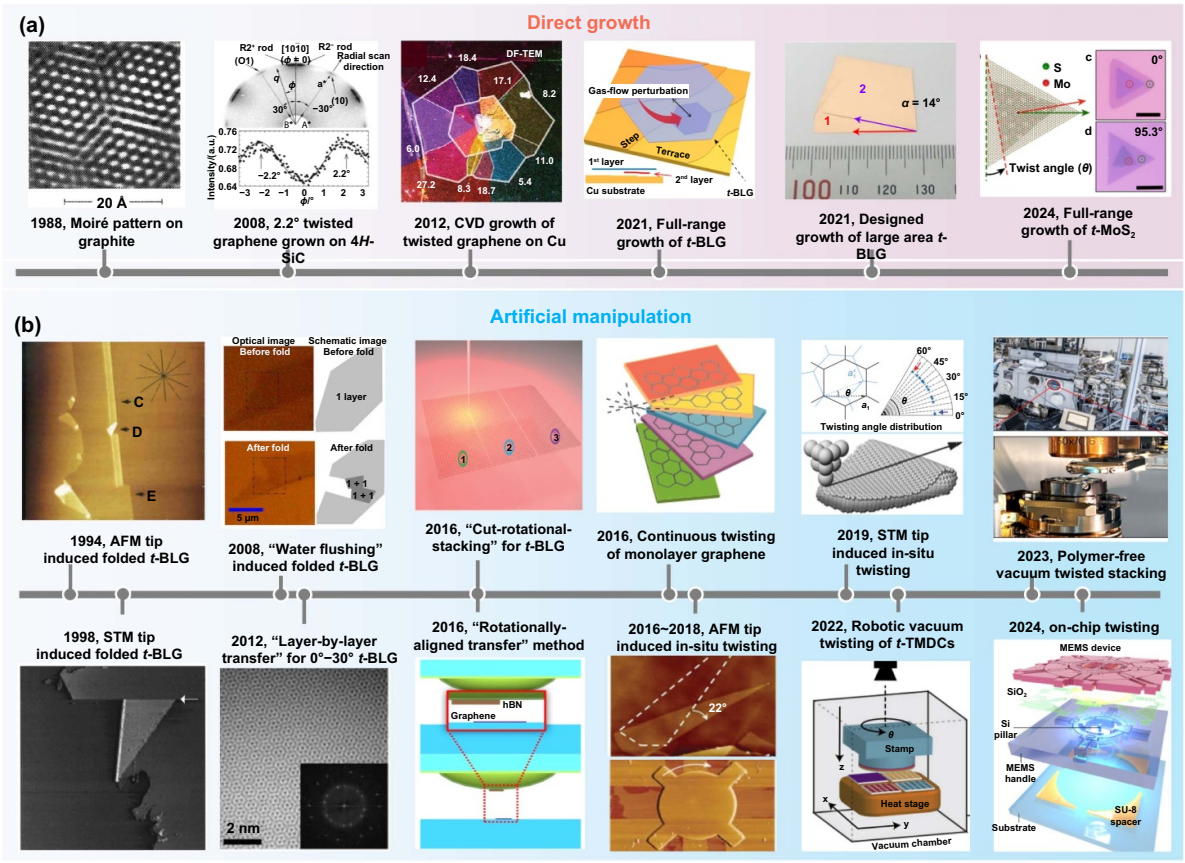

Figure 1. Historical development of fabrication technology for twisted 2D Moiré structures. (a) Preparing a twisted 2D superlattice via direct growth. (b) Preparing a twisted 2D superlattice by artificial manipulation. Reprinted from[26], with the permission of AIP Publishing. Reprinted figure with permission from[27], Copyright (2008) by the American Physical Society. Reprinted with permission from[28]. Copyright (2012) American Chemical Society. Reproduced from[31]. CC BY 4.0. Reproduced from[35], with permission from Springer Nature. Reproduced from[33]. CC BY 4.0. Reproduced from[36], with permission from Springer Nature. Reprinted from[37], with the permission of AIP Publishing. Reprinted figure with permission from[38], Copyright (2008) by the American Physical Society. Reprinted figure with permission from[39], Copyright (2012) by the American Physical Society.[40] John Wiley & Sons. © 2016 WILEY-VCH Verlag GmbH & Co. KGaA, Weinheim. Reprinted with permission from[41]. Copyright (2016) American Chemical Society. Reproduced from[42], with permission from Springer Nature. Reprinted figure with permission from[43], Copyright (2016) by the American Physical Society. From[44]. Reprinted with permission from AAAS. From[45]. Reprinted with permission from AAAS. Reproduced from[46], with permission from Springer Nature. Reproduced from[47]. CC BY 4.0. Reproduced from[48], with permission from Springer Nature.

hexagonal system, while black phosphorus, MoO_3, and CrOCl belong to an orthogonal crystal system[20,73–76].

In general, a hexagonal Moiré pattern can be formed by stacking two layers of hexagonal 2D materials, as shown in Figure 2(a). For instance, *h*-BN and graphene are stacked, and three highly symmetric regions are formed, including AA, AB, and BA, as illustrated in Figure 2(d). In the AA stacking region, the atoms in the bilayers are highly aligned in the perpendicular direction, whereas they are misaligned in the AB and BA stacking regions. In *t*-BLG, the density of states (DOS) differs between AA and AB regions because of distinct interlayer coupling and band structures within the Moiré pattern. AA regions have strong coupling, leading to flat bands (especially near magic angles), high DOSs (sharp peaks/van Hove singularities), and localized electrons. AB regions have weaker coupling, resulting in more dispersive (Dirac-like) bands, a low V-shaped DOS near the Dirac point, and delocalized electrons. This spatial DOS modulation is key to the unique electronic properties of TBG[77,78]. Similarly, stacking TMDCs such as MoS_2 and WSe_2 at a 0° (H-type) twist angle produces AA, AB, and BA configurations. A 180° (R-type) twist angle, however, results in AA′, A′B, and AB stacking modes. Experimental observations confirmed distinct local electronic states between these two stacking types in twisted TMDC bilayers[79]. For example, in twisted $WS_2/MoSe_2$ bilayers, the interlayer distance and strain are greater at the AA position than at the AB and BA position[80]. Furthermore, the study indicates that the Moiré potential well for interlayer excitons is deeper at the AA position than at the AB or BA positions[81].

In the case of the orthogonal system, as shown in Figure 2(b), the specific twist angle also determines the overall

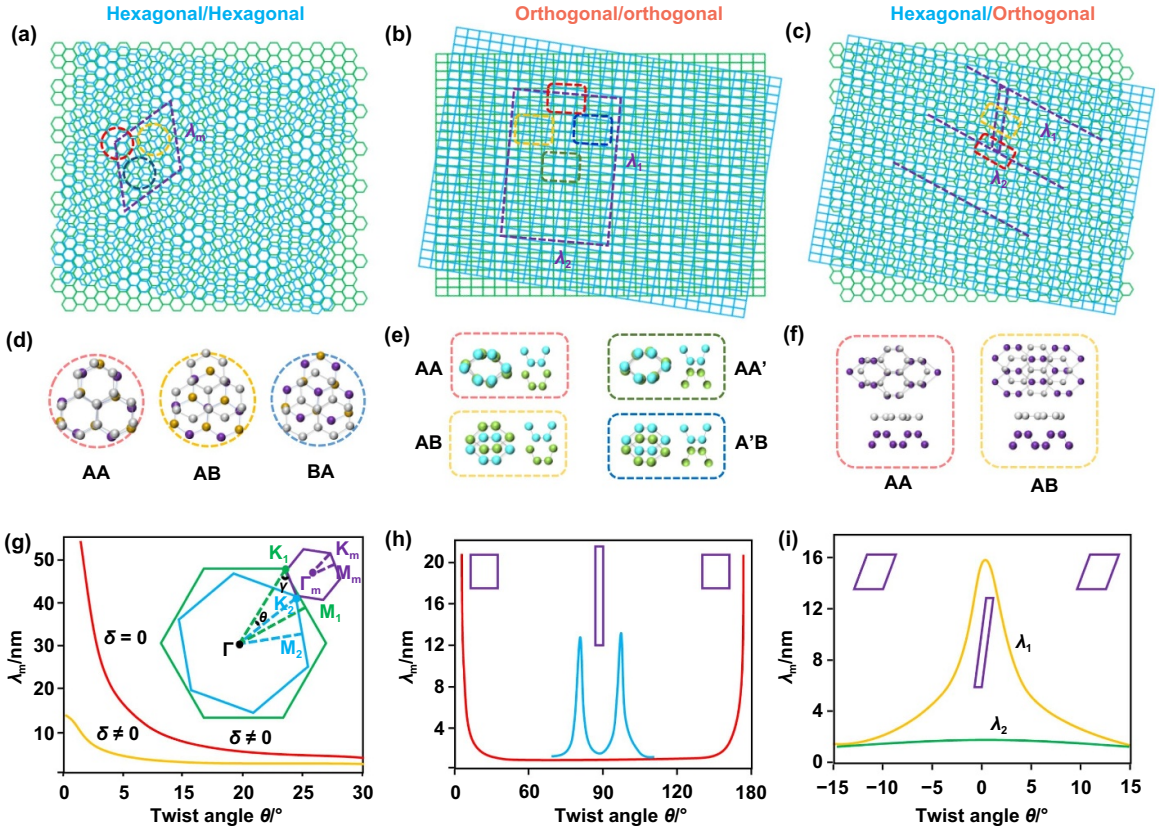

Figure 2. Moiré superlattice with a twisted stacking angle. (a) Hexagonal Moiré pattern produced by homo-hexagonal 2D lattices. (b) Rectangular Moiré pattern produced by homo-orthogonal 2D lattices. (c) Striped Moiré pattern formed by hetro-geometry consists of hexagonal and orthogonal 2D lattices. (d)–(f) Highly symmetric regions in the Gr/*h*-BN Moiré pattern, BP/BP Moiré pattern and Gr/BP Moiré pattern, respectively. (g) The periodicity and geometry of the hexagonal moiré superlattice; the red and orange lines represent the two layers of 2D materials with and without mismatch, respectively. The inserted figure depicts the minimum Brillouin Moiré superlattice composed of two hexagonal lattices in momentum space; the cyan line and green line represent 2D materials with a hexagonal lattice, and the purple line represents the obtained Moiré pattern. (h) The periodicity and geometry of the BP/BP Moiré superlattice; the red line indicates the rectangular Moiré pattern, and the blue line indicates the striped Moiré pattern. Reprinted from[82], Copyright (2022), with permission from Elsevier. (i) The periodicity and geometry of the Gr/BP Moiré superlattice; the green and yellow lines represent the two sides of the parallelogram. Adapted from[83], with permission from Springer Nature.

topological geometry of the Moiré pattern. For example, in addition to a rectangular Moiré pattern, a striped Moiré pattern appears at a certain twist angle in bilayer BP[84]. Compared with the hexagonal shape, the rectangle has reduced symmetry. Therefore, there are four kinds of high symmetry centers (AA, AA′, AB, and BA) in this Moiré system, as shown in Figure 2(e)[85]. In the AA (AA′) stacking region, the atoms in the bilayer are aligned vertically in the same (opposite) direction, while in the AB and BA stacking regions, the atoms are staggered in the same and opposite directions.

A particularly notable case arises when the constituent 2D materials belong to different crystal systems, and the morphology of the resulting Moiré patterns evolves with the twist angle. As shown in Figure 2(c), a striped Moiré pattern can be obtained in a heterojunction formed by hexagonal graphene and orthogonal BP[83]. This one-dimensional Moiré pattern has great potential in the anisotropic modulation of light, electricity, magnetism, and force[86,87]. In this striped Moiré system, there are two stacking modes (AA and AB), as depicted in Figure 2(f).

1.2. Moiré pattern periodicity

In addition to the geometric shape of the Moiré patterns, the length of the Moiré periodicity is also directly determined by the twist angle[88]. For example, in a hexagonal system, the minimum Brillouin zone of the elementary material lattice is hexagonal, as the insertion depicted in Figure 2(g). Given the twist angle of the 2D materials is θ, the unit cell parameters of the lower and upper layers are a and b, respectively, and the lattice mismatch rate is defined as $\delta = (b\text{-}a)/a$. Therefore, a new hexagonal minimum Brillouin zone of the Moiré pattern can be obtained, which is presented as a purple hexagon in Figure 2(g), and its vector in momentum space can be calculated as $\overrightarrow{K_1K_2} = \overrightarrow{\Gamma K_2} - \overrightarrow{\Gamma K_1}$. The size of periodicity in this Moiré geometry can be mathematically derived using a, b, and θ, and the final result is shown in Equation (1)[88,89]. The new Moiré pattern has a γ-angle deflection relative to the underlying material, and γ can be calculated via Equation (2)[90]. In homojunctions, $\delta = 0$, while heterojunctions generally have a certain lattice mismatch ($\delta \neq 0$). As illustrated in

Figure 2(g), the smaller the lattice mismatch is, the more sensitive the Moiré periodicity is to regulation by the twist angle[91]. Interestingly, in twisted 2D systems, many unique physical phenomena, such as atomic reconstruction and the emergence of flat bands, are concentrated in the small twist-angle region. A detailed discussion of these phenomena is presented in Section 1.3.

Compared with that of the hexagonal system, the symmetry of the orthogonal system is reduced, resulting in more complex variations in the Moiré systems, which will be discussed in detail in Section 1.3. As depicted in Figure 2(h), when the twist angle in twisted bilayer BP increases from 0° to 90°, the shape of the Moiré patterns transform from rectangular to striped[82]. When θ is near 0°, for each side a or b, it is equivalent to the case of no mismatch, and its Moiré pattern is a rectangle. The length and width of the rectangle obey the case of $\delta = 0$ in Equation (1). With the twist angle increasing, the length of Moiré rectangle becomes progressively smaller and is accompanied by a change in the aspect ratio. When θ reaches about 66°, the aspect ratio of the rectangle begins to increase significantly because the short side is much smaller than the long side, resulting in a visually striped Moiré pattern. The striped Moiré periodicity in this bilayer BP system reaches the highest at approximately 75° and disappears at around 84°. In the case of 90°, the lattice mismatch is the largest, and the subsequent periodicity is symmetrical with the previous 90°.

For the heterojunction formed by hexagonal and orthogonal 2D materials, a parallelogram-shaped Moiré pattern appears. As shown in Figure 2(i), in the Gr/BP heterostructure[83], there are two sets of lattice mismatches between the lattice cell of BP and graphene, namely, $\delta_1 = 0.34$ and $\delta_2 = 0.028$. Eventually, two Moiré periodicities, λ_1 and λ_2 will be obtained, which are the two sides of the Moiré parallelogram. In the small twist angle region ($\theta < 7°$), λ_1 is much larger than λ_2 because of the smaller lattice mismatch δ_2, resulting in a visually striped Moiré pattern. At larger twist angles ($7° < \theta < 15°$), λ_1 and λ_2 become close to each other, resulting in a small parallelogram Moiré pattern. This visually striped Moiré pattern is also observed in other systems, such as Cu_2Se/graphene[92], BP/WSe_2[93], and CrOCl/MoS_2[94].

$$\lambda_m(\theta,\delta) = \frac{(1+\delta)a}{\sqrt{2(1+\delta)(1-\cos\theta)+\delta^2}} \tag{1}$$

$$\tan\gamma = \frac{\sin\theta}{(1+\delta)-\cos\theta}. \tag{2}$$

1.3. Effects of twist angle on material properties

Topological analysis has demonstrated the direct influences of the twist angle on the geometric shape and period size of the Moiré pattern in twisted bilayer 2D materials. This not only introduces a new Moiré periodic potential field but also changes the local electronic interaction within a period[95]. Therefore, the twist angle is a crucial factor in modulating the physical properties of the 2D Moiré structure. Using bilayer graphene as an example, for small twist angles ($\theta < 1°$), weakly dispersive bands emerge at low energies, characterized by a high DOS near the Dirac point[96,97]. At the magic angle (∼1.1°), strong interlayer coupling creates ultra-flat bands near the Fermi level, leading to highly localized electrons (extremely high DOS). This massive enhancement of the DOS drastically amplifies electron−electron interactions, making correlation effects dominate over kinetic energy and enabling exotic quantum states. Another manifestation of interlayer coupling is the atomic reconstruction of the Moiré lattice, where the twist angle causes periodic arrangements of the AA, AB, and BA stacking modes[98]. When the twist angle is nearly zero (<2°), the lower energy associated with AB (BA) stacking modes results in area expansion of these regions, ultimately forming a distinctive periodic triangular pattern. For intermediate twist angles ($1° < \theta < 15°$), the band velocity near the Dirac points in both layers is expected to decrease, resulting in the formation of two saddle van Hove singularities (vHs) in the DOS distribution[99–101]. For larger angles ($15° < \theta < 30°$), the band structural characteristics of *t*-BLG at low energy are generally similar to those of its monolayer counterpart[102,103]. Table 1 summarizes the physical properties of different 2D Moiré superlattices classified according to their Moiré structural compositions and material types.

The hexagonal Moiré system has been the most extensively studied due to the rich variety of primitive materials. Since Jarillo-Herrero observed unconventional superconducting and correlated insulating phases in *t*-BLG with a magic angle of about 1.1°[23,77], many physical properties, such as magnetism[140,141], ferromagnetism[142,143], topological Chern insulators[144,145], Pomeranchuk effects[110], and intrinsic quantized anomalous Hall effects[112], have been discovered in magic-angle *t*-BLG. Outside the magic angle region, many fantastic properties are also found in other twisting cases, including correlated states, topological Hofstadter butterfly, photoelectric effect, orbital magnetic moment, and quasicrystals (listed and referenced in Table 1).

These findings highlight the angle-dependent diversity of physical properties in *t*-BLG and underscore the critical role of the twist angle in modulating these characteristics. In addition to the twisted homojunctions of bilayer graphene, 2D graphene-based twisted heterojunctions, such as graphene/h-BN, graphene/TMDCs, and graphene/BP, also demonstrate a range of distinctive properties. Additionally, as a broad class of 2D materials within the hexagonal system, TMDCs exhibit a wide spectrum of electronic properties, including metallic, semiconducting, and insulating behaviors, along with unique electrical, optical, magnetic, and thermal characteristics[18,146–148]. This suggests that TMDCs-based twisted bilayers could potentially display an even greater variety of properties.

Unlike highly symmetric 2D materials (e.g., graphene), orthorhombic-phase materials such as BP exhibit fundamentally distinct Moiré superlattice structures owing to their inherent low symmetry and pronounced intrinsic anisotropy. In such systems, the periodicity and symmetry of the resulting

Table 1. Physical properties in different 2D Moiré superlattice systems.

Structural composition	Materials composition	Twisted angle/°	Physical property	References
Hexagonal/hexagonal	Gr/Gr	0	Tunable band gap in AB stacking	[104]
		0.45	Hofstadter topology	[105]
		0.6	Terahertz photogalvanics	[106]
		0.79	WSe_2 stabilized superconductivity	[107]
		0.93	Superconductivity and Mott insulating state	[108]
		1.1	Superconductivity	[23]
			Correlated insulating state	[77]
			Magnetism	[109]
			Pomeranchuk effect	[110]
			Gate-defined Josephson junctions	[111]
			Intrinsic quantized anomalous Hall effect	[112]
		1.27	Superconductivity and Mott insulating state	[113]
		1.68	Orbital magnetic moment	[114]
		1.81	Photo responsible	[115]
		2	Odd integer quantum Hall states	[116]
		13	Selectively enhanced photocurrent	[117]
		1–15	Van Hove singularities	[101]
		30	Quasicrystal	[118]
	h-BN/h-BN		Tunable ferroelectricity	[119]
	Gr/h-BN		Second Dirac point	[120]
			Unexceptional band gap	[121]
			Hofstadter butterfly	[122]
			Topological currents	[123]
	Gr/TMDC		Flat band and correlated states	[124]
			Mini bands	[125]
			Spin–orbit coupling	[126]
	TMDC/TMDC		Topological insulators	[127]
			Superconductivity	[128]
			Quantum anomalous Hall effect	[129]
			Spin-textured Chern bands	[130]
			Ferroelectricity	[131]
			Light-induced ferromagnetism	[132]
			Atomic reconstruction	[133]
			Interlayer Moiré excitons	[81]
			One-dimensional Luttinger liquids	[134]
Orthogonal/orthogonal	BP/BP		Interlayer coupling effect	[135]
			Anisotropic Moiré optical property	[84]
			Resonant tunneling behavior	[136]
			Moiré impurities effect	[137]
	MoO_3/MoO_3		Phonon Polaritons	[138]
Hexagonal/orthogonal	Gr/BP		Spatially tailored pseudo-magnetic fields	[83]
	MoS_2/CrOCl		In-plane optical polarization	[94]
	WSe_2/BP		In-plane electronic polarization	[93]
	Bismuthene/BP-Bi		Topological edge states	[139]

Moiré pattern exhibit a strong dependence on both the magnitude and direction of the interlayer twist angle. This dependency generates a highly anisotropic Moiré potential and non-hexagonal Brillouin zones (e.g., rhombic or rectangular), substantially broadening the parameter space for control via twist orientation. The complexity of interlayer coupling arises from the spatial orientation dependence of atomic orbitals—exemplified by the d-orbitals in TMDs—rendering its strength highly sensitive to local atomic stacking configurations (AA, AB, SP, etc.) and specific twist parameters. At small twist angles, significant local atomic reconstruction occurs to minimize the system energy, forming distinct domains of high-symmetry stacking separated by domain walls. This reconstruction directly modulates the interlayer

coupling strength, band alignment, and bandgap characteristics, profoundly impacting the electronic transport and optical response properties. This is evidenced by phenomena such as anisotropic electrical conductivity modulation in twisted BP and photon polarization control in twisted MoO_3 bilayers[18,146–148]. Crucially, research on orthorhombic 2D materials and their heterostructures remains significantly less explored compared to their hexagonal counterparts, necessitating further in-depth investigation.

Lattice symmetry is further reduced in the hybrid hexagonal/orthogonal Moiré system, resulting in richer and more unique properties of the localized electronic states. Therefore, the Moiré superlattice exhibits strong angle-dependent in-plane polarizations and topological effects in photonics, electronics, and magnetism. In addition, owing to the different lattice systems, this hybrid lattice system may give rise to more unique properties that may not be found in a homo-lattice stacked system.

In conclusion, the twist angle is not merely a geometric parameter but also a fundamental control knob for the emergent properties of twisted 2D superlattices. In twisted bilayer graphene, sub-degree variations can reshape the electronic band structure, leading to bandgap renormalization, van Hove singularities, and the emergence of nearly flat bands at "magic angles," which underpin unconventional superconductivity and correlated insulating phases. In addition to graphene, TMD bilayers exhibit twist-dependent interlayer coupling and Moiré excitons, producing tunable optical responses and exciton funneling effects relevant for valleytronics and optoelectronic devices. In addition, low-symmetry 2D materials such as black phosphorus or MoO_3 display strongly anisotropic Moiré potentials, where the periodicity and electronic coupling depend sensitively on both the magnitude and direction of the twist angle, enabling modulation of electronic transport and photon polarization responses. More generally, the twist angle directly influences the effective lattice symmetry of the resulting Moiré pattern: small angular changes can alter rotational symmetry, modify selection rules, and lift degeneracies in electronic or excitonic states.

2. 2D Moiré fabrication

The novel physical phenomena observed in twisted stacking systems provide exciting opportunities for exploring the properties of 2D materials. Research in this area imposes stringent requirements on the precise fabrication of 2D material stacks, including the compatibility between different materials, the cleanliness of the transfer and stacking surfaces or interfaces, and the precise control of the twist angle. Currently, two primary approaches are employed for constructing twisted 2D materials: direct growth and artificial manipulation. This section provides an overview of several representative methods for fabricating twisted 2D materials, discussing their respective advantages and limitations.

2.1. Direct twisted growth

In the direct growth approach, the growth mode and underlying mechanism depend on the material type. Twisted 2D materials produced by this method exhibit high crystallinity and pristine interfaces, making them ideal for studying intrinsic properties. However, achieving bilayer 2D materials with tunable twist angles via direct growth remains challenging. The van der Waals (vdW) surface, characterized by low surface energy and an absence of dangling bonds, hinders the adsorption of precursor molecules necessary for secondary nucleation. As a result, many 2D materials are confined to a "self-limiting" monolayer growth mode. Furthermore, even when bilayer 2D materials are formed, high growth temperatures impose thermodynamic constraints that align stacking angles with crystal symmetry, limiting the range of twist angles. In the following sections, we explore the direct growth methods for twisted homojunctions, heterojunctions, and spiral superlattices in materials such as graphene, h-BN, and TMDCs. Special attention is given to twist nucleation, the critical step in the growth process. We systematically examine the factors influencing twist nucleation, including substrate properties, gas flow dynamics, precursors, and additives.

2.1.1. Twisted growth of graphene. Graphene, a widely studied 2D material, is synthesized using two methods: epitaxial growth on SiC (0001) substrates and CVD on metal substrates like Cu or Ni. In the SiC epitaxy process, high-temperature evaporation of silicon leaves behind carbon atoms that crystallize into graphene. By adjusting the temperature and growth time, graphene sheets ranging from a few to dozens of layers can be produced, typically adopting the AB (Bernal) stacking configuration owing to its energetic stability[149]. SiC substrates feature two types of atomic terminations: Si faces and C faces. In 2008, Hass et al. observed "rotational stacking faults" in graphene grown on C-face SiC, characterized by a 2.2° twist angle[27]. These findings, validated by low-energy electron diffraction (LEED) and x-ray azimuthal scans, are shown in Figure 3(a). Later, in 2010, Miller et al. reported 'double-moiré' patterns in trilayer graphene grown on SiC(0001), resulting from continuous twisting influenced by interlayer lattice strain[150]. These studies marked early efforts in directly growing twisted graphene.

Despite these advancements, only a few twist angles have been achieved in SiC epitaxial graphene, with limited control over the interlayer twist angles. Consequently, attention has shifted toward CVD as an alternative. CVD is a widely used in-situ growth method for producing large-area, high-quality monolayer 2D materials, including graphene, on transition metal substrates such as Cu and Ni[153]. However, two significant challenges remain for the CVD growth of twisted graphene: (1) the self-limiting growth mechanism, which complicates stable multilayer synthesis, and (2) difficulty in controlling interlayer twist angles owing to stacking energy equilibrium.

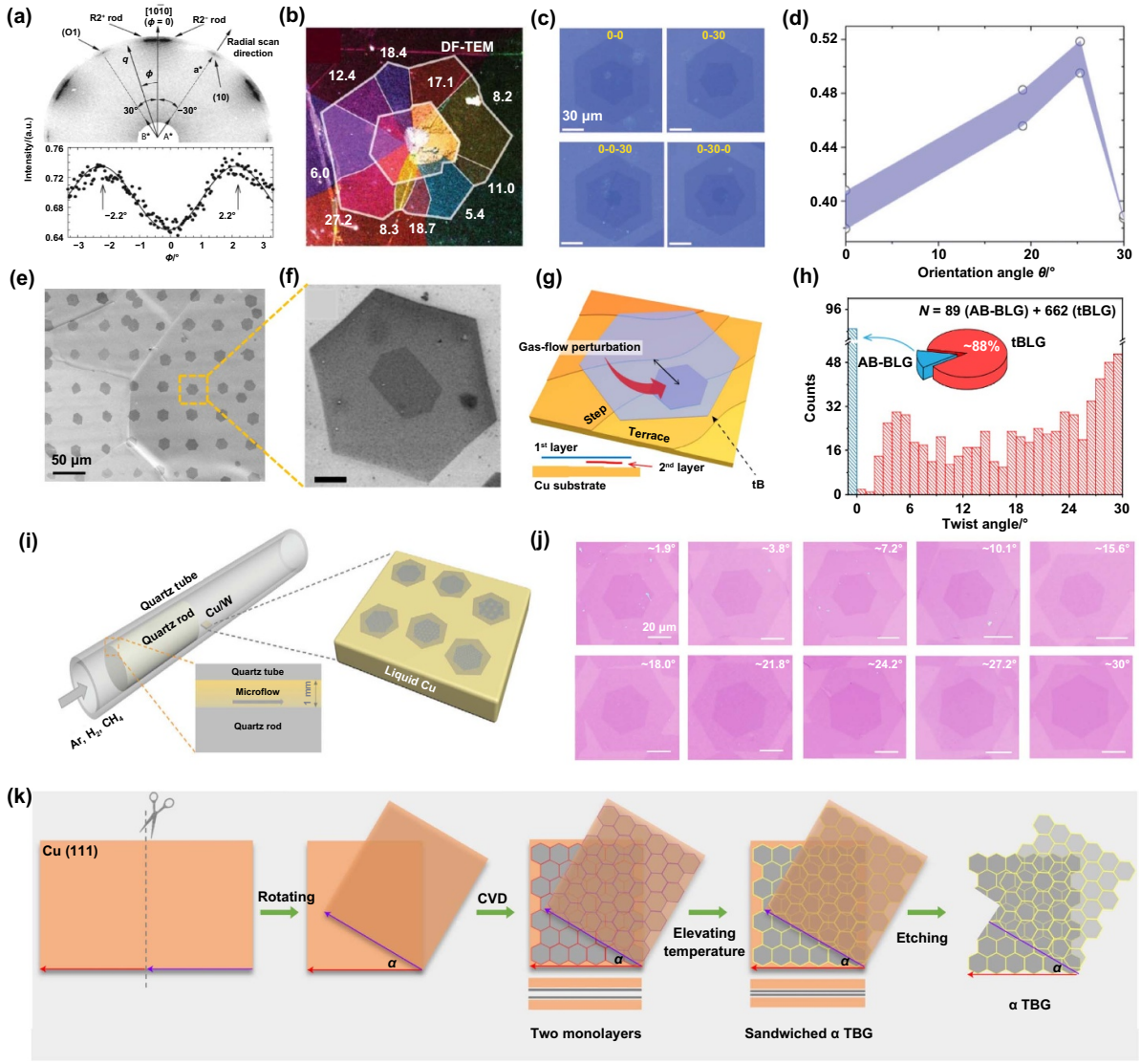

Figure 3. The *t*-BLG fabricated by the direct growth method. (a) LEED and x-ray azimuthal scans by growth of *t*-BLG by the ectopic nucleation strategy. Reprinted figure with permission from[27], Copyright (2008) by the American Physical Society. (b) Dark field TEM image of polycrystalline *t*-BLG grown on Cu. Reprinted with permission from[28]. Copyright (2012) American Chemical Society. (c) 0° and 30° grown twisted multilayer graphene. (d) Calculated interface energy of *t*-BLG on Cu.[151] John Wiley & Sons. Copyright © 2014 WILEY-VCH Verlag GmbH & Co. KGaA, Weinheim. (e)–(f) The *t*-BLG array grown on Cu by using patterned PMMA as a seed. Reprinted with permission from[152]. Copyright (2013) American Chemical Society. (g)–(h) Ectopic nucleation of *t*-BLG on Cu (g) and the twist angle distribution histogram (h). Reproduced from[31]. CC BY 4.0. (i)–(j) Mono-nucleation of *t*-BLG on liquid copper (i) and optical microscope image (j).[32] John Wiley & Sons. © 2023 Wiley-VCH GmbH. (k) "Pre-stacked substrate-angle replication" approach for the growth of twisting designable *t*-BLG. Reproduced from[35], with permission from Springer Nature.

Over the past two decades, considerable efforts have focused on angle-controllable twisted graphene synthesis via CVD. In 2012, researchers discovered that bilayer graphene with various twist-angle domains could be grown on polycrystalline Cu substrates[154–157]. Figure 3(b) illustrates the grain boundaries with different twist angles marked for each domain[28]. To achieve single-crystalline twisted graphene, efforts have shifted to single-crystalline Cu substrates. Yan et al. successfully grew bilayer and trilayer graphene with single-crystal domains on Cu foil, where the interlayer angles predominantly exhibited 0° and 30° orientations, as shown in Figure 3(c)[151]. The first-principles calculations in Figure 3(d) revealed that these orientations arise from a lower interface energy during nucleation, highlighting the importance of controlling the nucleation kinetics. To facilitate multi-oriented nucleation, Lu et al. patterned PMMA seeds on single-crystalline Cu foil, enabling the growth of single-crystalline *t*-BLG arrays with varied twist angles, as depicted in Figure 3(e)[152]. The hexagonal outlines of the primary and secondary layers in Figure 3(f) confirm the single-crystalline nature of each domain, with twist angles distinct from their orientations.

However, as shown in Figures 3(b), (c), and (f), multilayer graphene typically grows homonuclearly, resulting in symmetrical lateral growth that limits the variety of twist angles. Breaking this symmetry requires controlling the nucleation kinetics. In 2021, Sun et al. achieved ectopic nucleation by introducing gas turbulence during growth, enabling the synthesis of *t*-BLG with a wide range of twist angles, as shown in Figure 3(g)[31]. This approach resulted in a high *t*-BLG domain yield of 88%, as shown in Figure 3(h). Additionally, Liu et al. recently developed a local space-confined in-situ CVD technique for mono-nucleation of *t*-BLG on liquid Cu substrates, as shown in Figure 3(i). This method produced *t*-BLG with twist angles ranging from 0° to 30°, as demonstrated by the optical microscopy images in Figure 3(j)[32]. The introduction of a narrow gap between a quartz tube and rod confined precursor collisions, generating activated carbon intermediates that favored a thermodynamically unstable twisting growth mode.

Despite these advances, the twist angles of *t*-BLG synthesized via either heterotopic or homotopic nucleation remain randomly distributed. Achieving precise control over twist angles has emerged as a critical goal. Recently, Liu et al. introduced a "prestacked substrate-angle replication" method, enabling designable growth of large-area *t*-BLG[35]. As illustrated in Figure 3(k), by pre-folding single-crystal Cu foil at a desired angle, graphene grown epitaxially on the Cu (111) surface replicated the folding angle during high-temperature growth. After wet transfer, *t*-BLG with predetermined angles was obtained, providing a novel bottom-up approach for fabricating twisted 2D materials.

2.1.2. Twisted growth of 2D materials beyond graphene. For the growth of twisted 2D heterostructures beyond *t*-BLG, such as Gr/h-BN, TMDC/Gr, and h-BN/TMDC heterojunctions, a "two-step growth" method is commonly employed. In this approach, the first 2D material layer is synthesized via CVD and serves as a substrate for subsequent layer growth. Like those of bilayer graphene, the twist angles between these 3- or 6-fold symmetric materials are typically 0°, 30°, or 60°, aligning to minimize stacking energy. For example, Song et al. utilized prefabricated nucleation sites to sequentially grow h-BN and graphene on a Cu (111) substrate, achieving a twist angle of 0° between h-BN and graphene[158]. Likewise, achieving twisted TMDC/Gr and h-BN/TMDC heterojunctions through the "two-step growth" method is challenging. As shown in Figures 4(a) and (b), MoS_2 grown on graphene and WS_2 on h-BN tend to form with preferred orientation angles of 0° and 60°[159,160]. This method generally yields highly oriented bilayer structures, as illustrated in Figure 4(c), with NbS_2/MoS_2 single-crystal flakes in identical orientations[161]. These examples highlight that while the "two-step growth" method is versatile for synthesizing 2D heterojunctions, it is unsuitable for producing heterolayers with specific twist angles. The spontaneous alignment during nucleation, driven by the stacking energy and crystal symmetry, underscores the need for more precise control during CVD synthesis.

Following the discovery of graphene and *t*-BLG synthesis, the rapid development of TMDC materials and the emergence of twistronics have made constructing bilayer TMDCs with tunable twist angles a key challenge. In 2014, Liu et al. demonstrated that CVD-grown bilayer MoS_2 typically exhibited twist angles of 0°, 15°, and 60° under standard growth conditions[163]. However, for nearly two decades, the direct synthesis of twisted TMDCs (*t*-TMDCs) with a wider range of angles has remained elusive. This limitation was finally overcome in 2024, when two research groups independently reported methods for directly synthesizing *t*-MoS_2 with arbitrary twist angles. Xu et al. introduced a reconfigured nucleation CVD strategy assisted by NaCl, enabling the direct growth of bilayer MoS_2 with arbitrary twist angles, as shown in Figure 4(d)[33]. This process involves single-point nucleation, as confirmed by the optical microscopy results in Figures 4(e) and (f). The confined space and NaCl-assisted nucleation significantly increased the yield of twisted bilayer MoS_2 to 17.2%, achieving discrete full-angle coverage, as illustrated in Figures 4(g) and (h). A higher salt ratio provided more precursors and facilitated non-equilibrium nucleation under turbulent gas flow, producing a variety of twisted bilayer MoS_2 structures. Simultaneously, Zhou et al. employed a flow-perturbation CVD method to directly grow *t*-MoS_2 with diverse twist angles[34]. These results corroborated Xu's findings, emphasizing the sensitivity of *t*-MoS_2 formation to gas flow patterns. They further demonstrated control over homo-site and hetero-site nucleation by adjusting the gas flow program. Notably, a commensurate twist angle of approximately 22° in the homo-site nucleation accounted for 16% of the structures, attributed to its low formation energy.

Beyond hexagonal twisted materials such as *t*-BLG and *t*-MoS_2, researchers have begun exploring the direct growth of tetragonal twisted 2D materials. In 2024, Liu reported a precursor-regulated CVD method for high-quality twisted multilayer BiOCl[162]. By alternately introducing H_2O and O_2 precursors, secondary nucleation with a twist angle on the underlying BiOCl was achieved. As shown in Figure 4(i), the resulting twisted BiOCl exhibited large lateral sizes, high crystal quality, and twist angles ranging from 10° to 42°. Density functional theory calculations revealed that polar H_2O adsorption on the BiOCl (100) surface caused stable atomic dislocations during initial nucleation, enabling the formation of rotated layers. This precursor-regulated approach offers a novel pathway for synthesizing twisted 2D materials.

2.1.3. Spiral growth of the multilayer 2D Moiré structure. Unlike twisted bilayer superlattices, continuous multilayer twist systems exhibit more complex Moiré patterns, interlayer coupling, charge transfer, and optoelectronic properties[164–166]. However, fabricating such structures poses significant challenges, particularly in achieving continuous multilayer twisted 2D materials with discrete layers. To date,

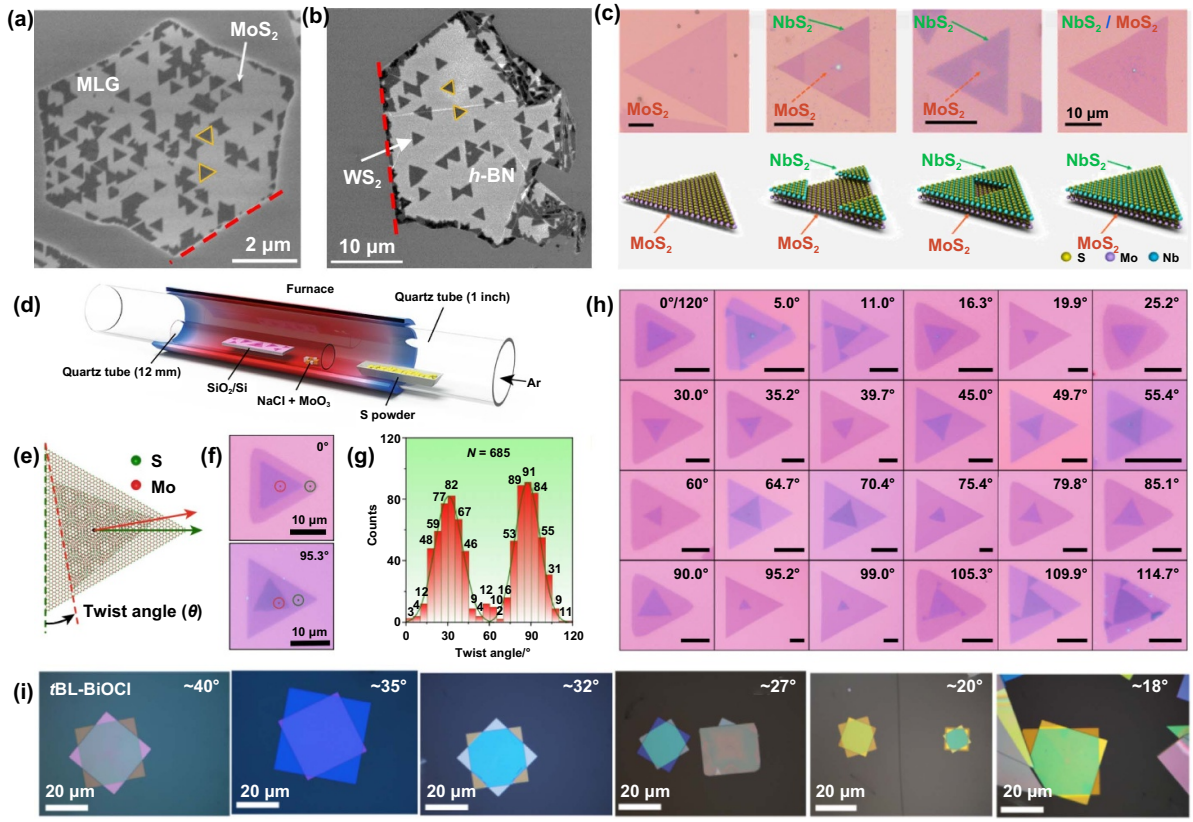

Figure 4. 2D Moiré structure beyond *t*-BLG fabricated via the CVD method. (a) Highly aligned MoS_2 grown on graphene. Reprinted with permission from[159]. Copyright (2015) American Chemical Society. (b) Highly aligned WS_2 grown on h-BN. Reprinted with permission from[160]. Copyright (2014) American Chemical Society. (c) The optical image (top) and model diagram (bottom) of highly aligned NbS_2/MoS_2 heterojunctions. Reprinted with permission from[161]. Copyright (2018) American Chemical Society. (d) CVD growth of *t*-MoS_2. (e)–(f) Twisted nucleation diagram and (e) optical microscope image (f) of bilayer MoS_2. (g)–(h) Twist angle distribution histogram (g) and optical images (h) of twisted bilayer MoS_2 ranging from 0° to 120°. Scale bar, 10 μm. Reproduced from[33]. CC BY 4.0. (i) Optical microscope image of *t*-BL BiOCl. Reprinted from[162], Copyright (2024), with permission from Elsevier.

no reliable method exists to grow continuous multilayer twisted 2D materials with clearly separated layers.

As shown in Figure 5(a), screw-dislocation-driven (SDD) spiral growth offers a unique approach to producing multilayer Moiré superlattices, though the layers are not discrete[167]. This method provides a versatile and high-throughput technique to fabricate spiral superlattices with four-dimensional (4D) control over *x, y, z*, and θ (twist angle). While the spatial coordinates (*x, y, z*) can be controlled by adjusting chemical kinetic parameters, tuning the twist angle (θ) requires leveraging non-Euclidean substrates.

Typically, the SDD growth mechanism occurs on planar Euclidean substrates, where screw dislocations form edge-aligned triangular spirals, as illustrated in Figure 5(b)[168]. However, when spirals grow on conical surfaces, they follow the substrate's curvature, resulting in consistent twist angles between layers, as illustrated in Figures 5(c) and (d)[168]. Steeper cone inclinations promote the formation of supertwisted spirals with larger twist angles. The interaction between the screw dislocation core and the non-Euclidean substrate is key to controlling the twist angle.

Spirals, including aligned spirals and supertwisted spirals, represent a novel type of Moiré superlattice. The twist angle between adjacent spiral layers can be modulated by strain or substrate properties. For example, Figure 5(e) shows an aligned WS_2 spiral grown on a flat substrate[169]. Here, the SDD mechanism introduces strain, producing a small twist angle between layers that is challenging to detect optically but measurable via STM. Figure 5(f) presents an atomic-resolution STM image of an aligned three-layer WS_2 spiral, where the Moiré pattern arises from strain-induced twist alignment[167]. In contrast, supertwisted spirals with large twist angles can be synthesized on non-Euclidean substrates. As depicted in Figures 5(g) and (h), these larger angles are clearly visible in both optical and AFM images[169].

As summarized in Figure 5(i), numerous 2D spiral materials have been successfully synthesized, creating a new library of twisted materials[170–179]. Compared to the growth methods for *t*-BLG or *t*-TMDCs, the spiral structure offers superior crystallinity and cleanliness while enabling high-throughput production of continuous multilayer twist structures—something previously unachievable. Consequently, spiral

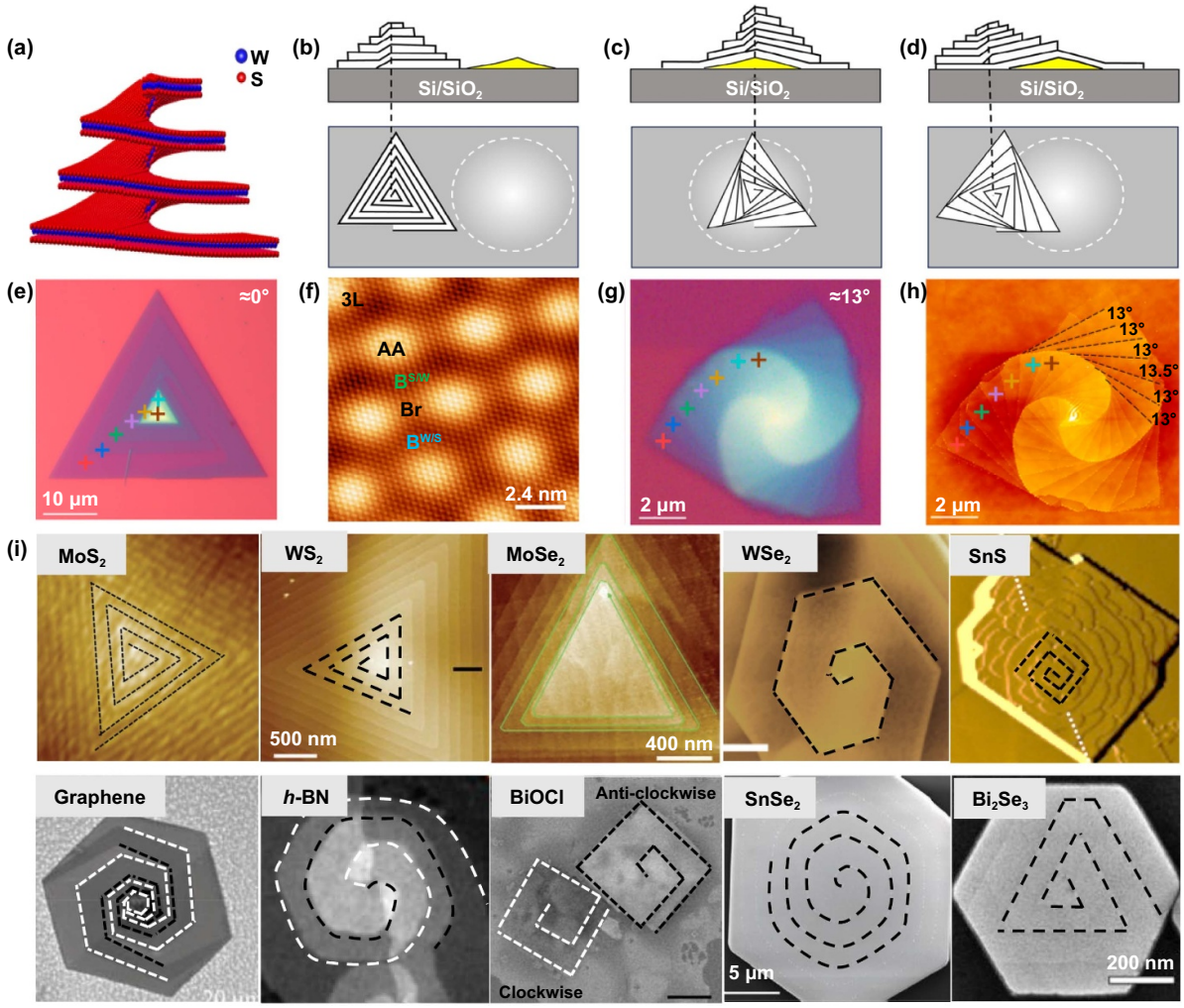

Figure 5. Spiral multilayer twisted 2D Moiré structure fabricated via the CVD method. (a) Perspective view of the schematic of a spiral WS_2 nanosheet. Reprinted with permission from[167]. Copyright (2022) American Chemical Society. (b) A flat substrate surface yields aligned spirals. (c)–(d) The uneven substrate surface yields left-handed or right-handed, supertwisted spirals. From[168]. Reprinted with permission from AAAS. (e)–(f) The optical microscope image (e) and STM image (f) of aligned spiral WS_2. Reprinted with permission from[169]. Copyright (2024) American Chemical Society. Reprinted with permission from[167]. Copyright (2022) American Chemical Society. (g)–(h) The optical microscope image (g) and AFM image (h) of supertwisted spiral WS_2. Reprinted with permission from[170]. Copyright (2024) American Chemical Society. (i) Different spiral twisted 2D structures.[171] John Wiley & Sons. © 2022 Wiley-VCH GmbH.[170] John Wiley & Sons. © 2024 Wiley-VCH GmbH.[172] John Wiley & Sons. © 2023 Wiley-VCH GmbH. Reprinted with permission from[173]. Copyright (2017) American Chemical Society. Reprinted with permission from[174]. Copyright (2021) American Chemical Society.[175] John Wiley & Sons. © 2022 Wiley-VCH GmbH. Reprinted with permission from[176]. Copyright (2019) American Chemical Society. Reproduced from[177]. CC BY 4.0.[178] John Wiley & Sons. © 2016 WILEY-VCH Verlag GmbH & Co. KGaA, Weinheim.[179] John Wiley & Sons. © 2014 WILEY-VCH Verlag GmbH & Co. KGaA, Weinheim.

Moiré superlattices are poised to significantly advance twistronics and optics research and applications.

2.2. *Transfer and twisted assembly*

Direct growth can produce Moiré structures with ultra-clean interfaces, but this approach faces several challenges in constructing twisted 2D superlattices: (1) achieving twisted nucleation requires complex and precise control of growth parameters, with the strategy further constrained by the varying growth modes and conditions of different materials; (2) the random distribution of twist angles makes it difficult to obtain samples with customized angles; and (3) the limited sample size (<100 μm) restricts large-area applications in future twistronics. An alternative and more widely adopted method is mechanical transfer and twist assembly, where 2D materials are isolated as building blocks and vertically stacked at predefined angles. This approach overcomes the limitations of size and the randomness of twist angles and offers broad applicability for fabricating twisted 2D structures.

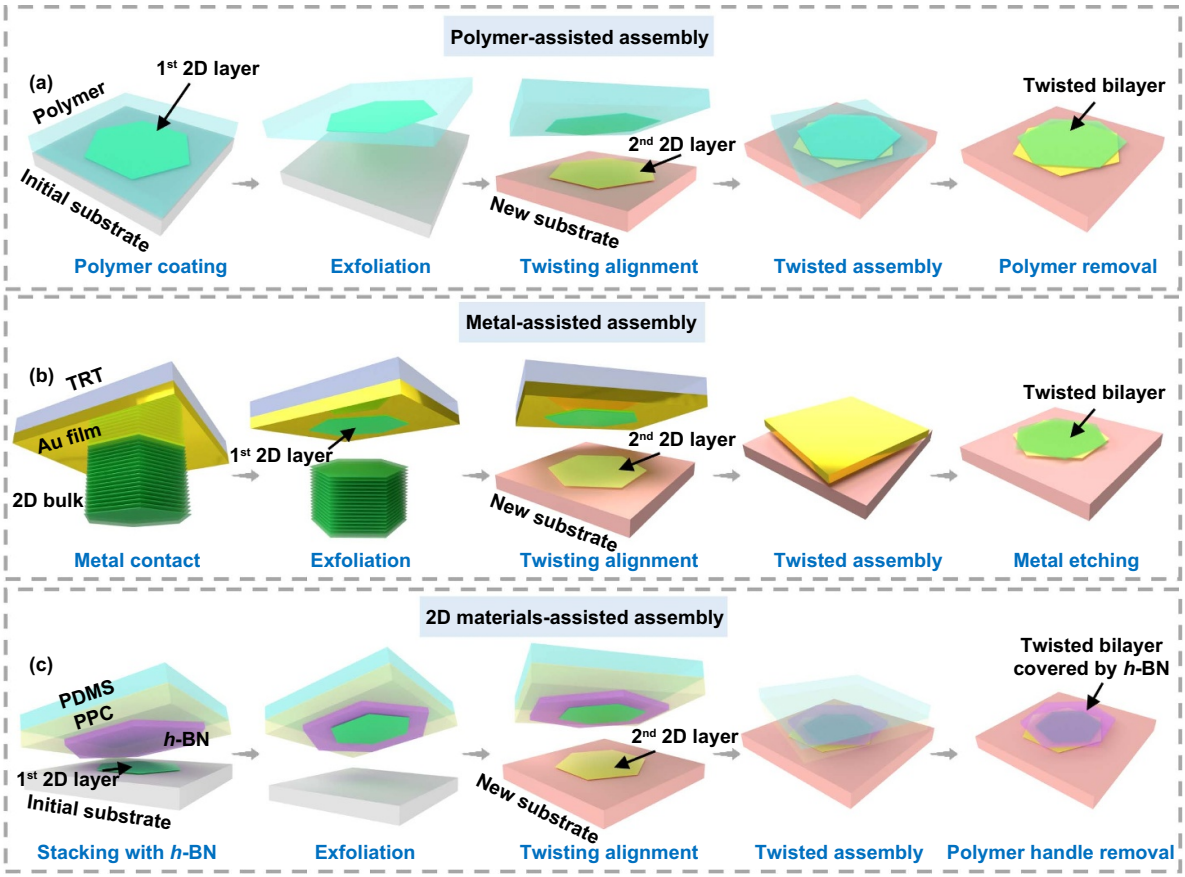

Figure 6. Transfer and twisted assembly methods. (a)–(c) Scheme of polymer-assisted (a), metal-assisted (b), and 2D material-assisted (c) transfer and twisted assembly processes.

2.2.1. Transfer and twisted assembly methods. Since monolayer graphene was first isolated and transferred onto a SiO_2/Si substrate via Scotch tape, clean transfer techniques for 2D materials have become crucial for property investigations and device applications[1,180]. In this process, 2D materials are mechanically peeled from the growth substrate and transferred to the target substrate using a transfer medium, which is later removed by etching or dissolving[181–183]. As shown in Figure 6, transfer methods are categorized based on the transfer medium: polymer-assisted wet transfer, metal-assisted semi-dry transfer, and 2D material-assisted pure dry transfer. The assembly of twisted 2D materials builds upon these techniques, essentially involving a controlled sequential transfer process. Different transfer media interact uniquely with 2D materials, leading to variations in the defect density, contamination, and uniformity of the resulting Moiré superlattice.

Polymer-assisted transfer involves the use of polymers such as PMMA or PDMS as support layers, as depicted in Figure 6(a)[184–186]. The main steps are as follows: (1) spin coat or laminating polymers such as polymethyl methacrylate (PMMA) or polydimethylsiloxane (PDMS) on the surface of the 2D material; (2) separate the 2D material from the substrate by etching the substrate or wedging water molecules into the interface; (3) with the support of the polymer, laminate the peeled 2D material to another layer of the prepared 2D material surface at a certain angle; and (4) finally, remove the polymer by dissolving or thermally releasing it. This method is widely applicable and suitable for large-area twisted structures. However, polymer residues, bubbles, and wrinkles can cause contamination and non-uniform stress, deforming the Moiré pattern. In addition to PMMA and PDMS, a variety of organic materials, such as polyvinyl alcohol (PVA)[187], polystyrene (PS)[188], cellulose carbonate (CA)[189,190], polyvinyl pyrrolidone (PVP)[191] and polypropylene carbonate (PPC)[192], have also been developed as transfer layers in recent years in pursuit of a cleaner stacking interface.

Metal-assisted transfer uses metals such as Au or Ag to facilitate the process, as shown in Figure 6(b)[193–197]. The steps include the following: (1) A pre-deposited metal film is stacked on the surface of the 2D material, or a metal film is directly evaporated onto the surface of the 2D material; (2) a single layer of 2D material can be peeled off to the metal surface; (3) the peeled single layer of 2D material is bonded to the surface of another 2D material at a certain twist angle; and (4) finally, the metal medium is removed by an etching solution. This method is particularly effective for TMDCs because of their strong metal interactions. For instance, Huang et al. demonstrated the transfer of various 2D chalcogenides and halides using Au[195]. While organic contamination is minimized, this approach introduces metal ion residues

and etchant-related impurities. Notably, metal-assisted transfer supports ultra-clean, vacuum-compatible assembly[47,198], making it suitable for certain high-precision applications, which will be discussed in detail in Section 2.2.4.

2D material-assisted transfer is also known as vdW interaction transfer. van der Waals materials such as h-BN can be used as transfer media to pick up and transfer 2D materials because of their strong interactions[180]. This method is often used for the transfer and encapsulation of monolayer and twisted bilayer graphene[180,199,200]. The basic steps are shown in Figure 6(c): (1) PDMS is used as the support layer, PPC is used as the adhesion layer, and the h-BN sheet is first selected as the transfer layer; (2) h-BN is attached to the surface of the target 2D material; (3) at a relatively low temperature (40 °C), h-BN can peel off the target 2D material from the SiO_2/Si substrate; (4) the selected 2D material is attached to the surface of another 2D material at a certain angle; and (5) at a relatively high temperature (110 °C), the heat-softened PPC can be peeled off from the h-BN surface, leaving the twisted 2D material encapsulated by h-BN on the substrate. This technique avoids contact with organic materials or solutions, making it the cleanest method for assembling twisted 2D materials. It is the preferred approach for studying electromagnetic transport properties and is compatible with glove box and vacuum operations, enabling the assembly of air-sensitive materials. However, the limited size of h-BN (<100 μm) constrains its application to large-scale twistronics.

2.2.2. Alignment principle and twist angle control. The interlayer rotation angle (θ) is a critical parameter in the preparation of Moiré superlattices, as it directly influences their period, structure, and properties. Precise control of θ during the transfer and assembly process is essential for accurate fabrication of 2D Moiré superlattices. Given variations in material type, preparation methods, and morphology, selecting an appropriate alignment technique is vital for achieving this precision. Typically, the alignment process is performed on a 4D transfer stage, as illustrated in Figure 7(a), which allows for relative movement in three axes (*x, y, z*) and rotation (θ) between two films[56]. The upper 2D material, supported by a polymer layer, is attached to a transparent glass sheet for real-time observation via a long-working-distance microscope. Two primary alignment methods are commonly used to control the twist angle: reference straight edge alignment and tear and rotational stacking. Each method offers varying levels of accuracy.

In "reference straight edge alignment", the straight edge refers to the edge of the 2D materials. These edges may be naturally formed in the 2D crystal or artificially fabricated. For instance, in C_3-symmetric materials such as CVD-grown TMDCs, the triangular morphology corresponds to armchair (AC) or zigzag (ZZ) crystal edges. When two triangles are stacked, the interlayer twist angle (θ or $\theta + 60°$) reflects the relative orientation of the crystals, as shown in Figure 7(b). This approach is commonly applied to twist-angle homojunctions or heterojunctions of TMDCs, as shown in Figure 7(c)[71]. In addition to naturally grown edges, artificial cutting and patterning can be used to create reference lines for twist-angle determination, as described in Figure 7(d). For example, patterned straight edge alignment has been employed to fabricate *t*-BLG and *t*-MoS_2 (Figure 7(e))[40,197,205]. Alternatively, crystal edges formed along principal crystallographic axes (PCAs) after mechanical exfoliation, such as the dashed lines in Figures 7(f) and (g), can also serve as alignment references[201]. Additionally, these crystallographic axes orientations (AC or ZZ) of TMDC crystals can be detected by second harmonic generation (SHG), which is a nonlinear optical response sensitive to crystal orientation under polarized laser irradiation, as illustrated in Figure 7(h)[202,206]. This method is suitable for TMDC-based homojunctions and heterojunctions. For example, 0.5°-twisted WSe_2/WS_2 heterostructures have been achieved using this technique, as shown in Figure 7(i)[72]. Recently, Shen et al. developed vacuum thermocompression bonding transfer technology and the 'wafer flat alignment' strategy to achieve wafer-scale Moiré superlattice preparation[203]. As illustrated in Figures 7(j)–(m), since MoS_2 and the growth substrate Al_2O_3 maintain a strict epitaxial relationship, when two MoS_2/Al_2O_3 wafers are stacked face to face, the angle between the wafer flats is the angle between the MoS_2 layers. This hard contact transfer process greatly reduces the material deformation caused by traditional polymer-assisted transfer, thereby improving the accuracy and uniformity of the Moiré superlattice. The accuracy of the reference straight edge alignment schemes mentioned above depends largely on the size and shape of the straight edge of the material, as well as the resolution of the optical microscope. The alignment accuracy of these alignment strategies varies between 0.2° and 0.5°.

As shown in Figures 7(n)–(p), in the 'tear and rotational stack' alignment technique, a portion of the 2D material is picked up, rotated by a defined angle (θ), and stacked onto the remaining material to create a twisted homobilayer[204]. This technique leverages the consistent crystal orientation within a single 2D crystal flake and does not require straight edges or external markers. The precision of the twist angle depends solely on the rotation accuracy of the transfer stage, achieving a minimal error of ±0.1°.

2.2.3. Assembly of the multilayer twisted 2D Moiré structure. Spiral growth can produce continuous multilayer 2D materials with twisted angles, but the layers are not entirely discrete and have limited area sizes. Currently, the only method to create discrete multilayer twisted angles is through multiple artificial stacking processes. For instance, as shown in Figure 8(a), Kim et al. fabricated multilayer graphene with continuous twisting angles by cutting single-crystal monolayer graphene on a Cu surface into parallel pieces, aligning their straight edges, and performing multiple PMMA-assisted transfers[42]. This artificially stacked graphene system exhibits controllable chirality through variations in the stacking orientation and layer number, as depicted in Figure 8(b). Similarly, Liao et al. achieved

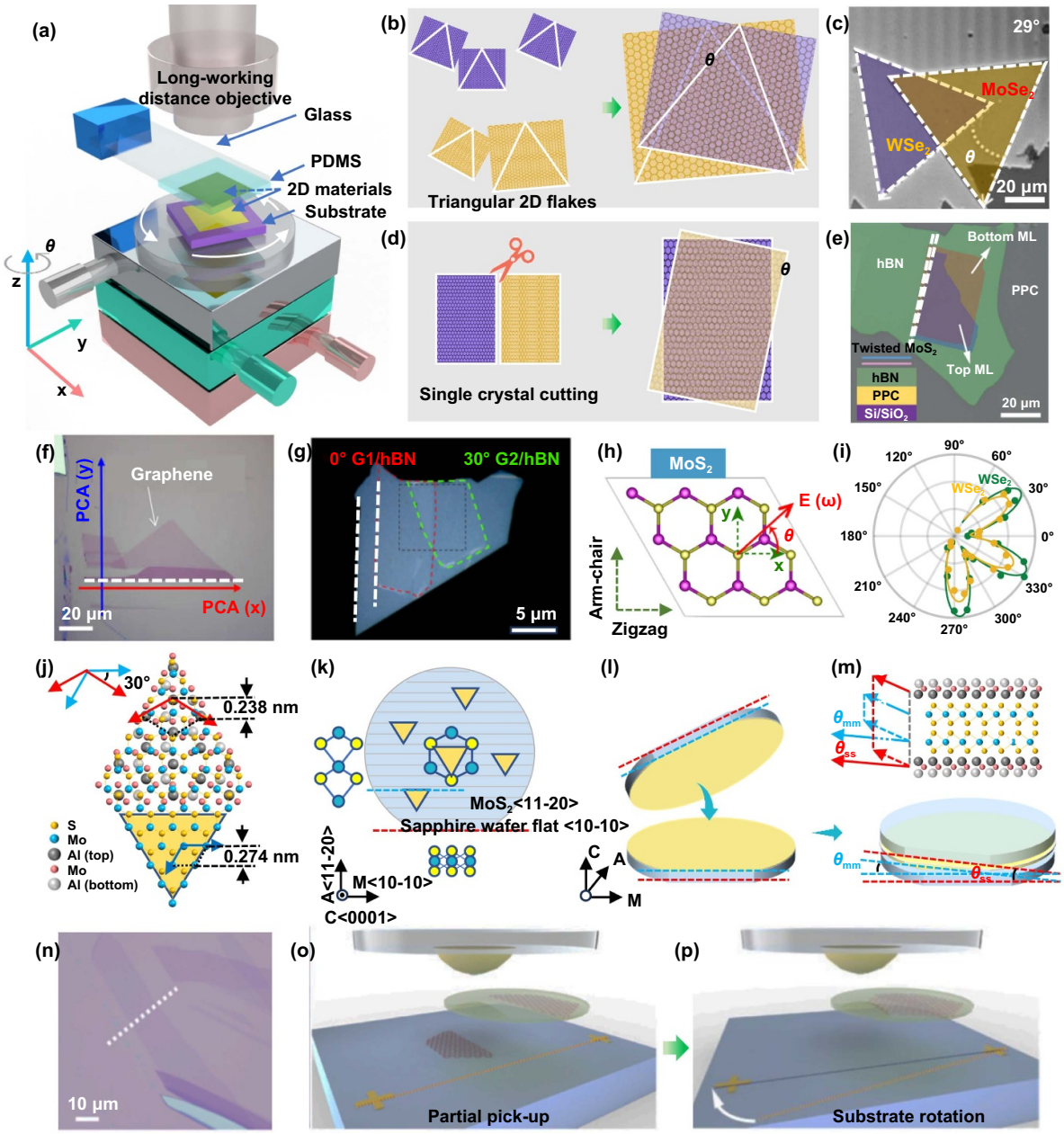

Figure 7. Alignment method for controlling the twist angle. (a) Schematic diagram of the 2D material transfer and alignment platform.[56] John Wiley & Sons. © 2025 Wiley-VCH GmbH. (b) Twisted stacking aligned by naturally formed crystal domain edges. (c) Optical microscope image of twisted $WSe_2/MoSe_2$. Reprinted with permission from[71]. Copyright (2017) American Chemical Society. (d) Twisted stacking aligned by the cutting edge. (e) Optical microscope image of twisted bilayer rectangular patterned MoS_2.[197] John Wiley & Sons. © 2024 Wiley-VCH GmbH. (f) Optical image of monolayer graphene with a straight graphite edge. (g) 0° and 30° stacked graphene/h-BN aligned by PCA. Reproduced from[201]. CC BY 4.0. (h) Armchair and zigzag edges in the MoS_2 crystal. Reprinted with permission from[202]. Copyright (2017) American Chemical Society. (i) Polarization-dependent SHG signals of the monolayer WSe_2 and WS_2. Reproduced from[72], with permission from Springer Nature. (j) Schematic diagram of the atomic epitaxy relationship between MoS_2 and C/A sapphire. The yellow triangle represents the MoS_2 crystal domain. (k) Orientation of MoS_2 crystal domains on a C/A sapphire substrate. (l) Face-to-face stacking of MoS_2/sapphire wafers along with the wafer flats. (m) Angular control based on sapphire wafer flats, resulting in a nearly rhombohedral stacked bilayer MoS_2.[203] John Wiley & Sons. © 2025 Wiley-VCH GmbH. (n) Optical image of a single graphene flake, which subsequently split into two sections along the dotted line. (o) The first section is detached from the substrate using a polymer handle. (p) The second section is detached from the substrate using the same handle. The substrate is rotated by a small angle between the two steps. Reproduced with permission from[204].

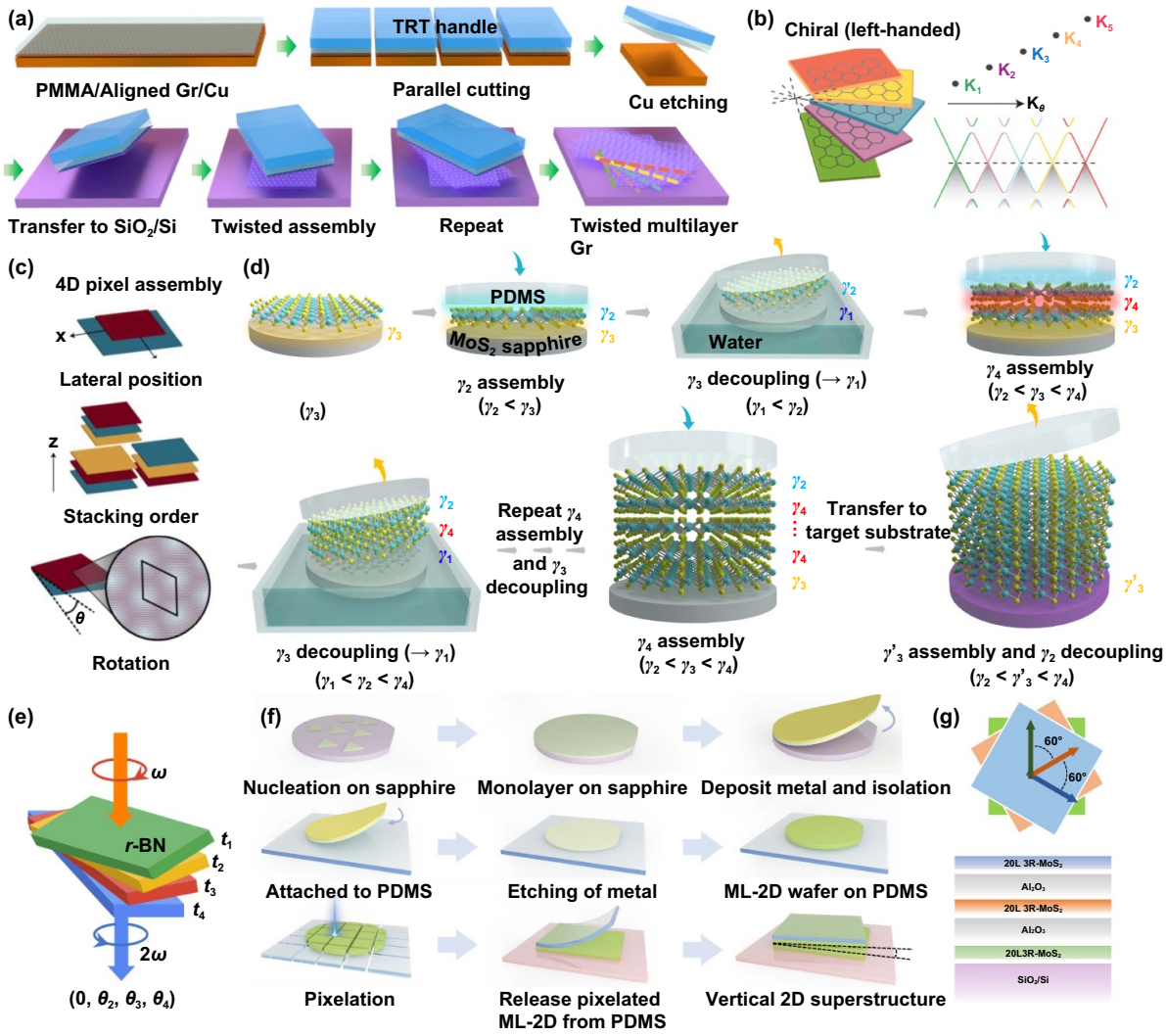

Figure 8. Artificial assembly of twist angle multilayers. (a) PMMA-assisted assembly of chiral graphene with continuous twist angles. (b) Schematics of chiral multilayer graphene and their respective band structures. Reproduced from[42], with permission from Springer Nature. (c) Robotic four-dimensional pixel assembly process. Reproduced from[46], with permission from Springer Nature. (d) Water-assisted van der Waals decoupling and reassembly for multilayer twisted TMDCs.[56] John Wiley & Sons. © 2025 Wiley-VCH GmbH. (e) Continuously stacked thick r-BN film. Reprinted figure with permission from[207], Copyright (2023) by the American Physical Society. (f) Metal- and PDMS-assisted fabrication of twisted multilayer thick MoS_2. (g) MoS_2/Al_2O_3 hybrid twisted superlattice. Reproduced from[57]. CC BY 4.0.

angle-controllable bilayer and tri-layer twisted MoS_2 using a PDMS-assisted multiple transfer method[205].

In PMMA- or PDMS-assisted transfer processes, each additional layer involves a transfer and release step, which introduces interlayer contamination. Such contamination accumulates with successive transfers. To address this issue, Mannix et al. developed a robotic 2D material-assisted assembly process, as shown in Figure 8(c)[46]. This method uses MoS_2 as a transfer medium for subsequent layers within a vacuum environment, which is controlled via mechanical programming, thereby minimizing contamination. Angle control in this process employs the "tear-and-rotational-stack" technique described in Section 2.2.2. This method also enabled the observation of atomic reconstruction in twisted four-layer WS_2 at high twist angles ($\geqslant 4°$). Recently, Shen et al. developed a water-assisted van der Waals force decoupling and recombination scheme for the rapid assembly of large-area multilayer twisted TMDCs. As shown in Figure 8(d), this scheme also avoids the contamination of interlayer organic matter and greatly improves the assembly efficiency[56]. Aligned by manually cutting straight edges, as mentioned in 2.2.2, controllable circular polarization activity was observed in the multilayer twisted TMDC system.

Beyond single-layer continuous twisting, the continuous stacking of thick-layer 2D materials can also regulate their properties. For example, in 2D nonlinear optical crystals such as rhombohedral boron nitride (r-BN) and 3 R-MoS_2, thickness-induced phase mismatches limit exponential increases in the SHG intensity. Hong et al. demonstrated that interlayer twist angles in 2D materials generate a nonlinear geometric phase, compensating for phase mismatches in thick layers[207]. As shown in Figure 8(e), continuously

twisted r-BN films exhibit enhanced SHG with a conversion efficiency of ∼8% and controllable polarization, which traditional crystals cannot achieve. Similar multilayer twisted stacking to achieve phase matching in nonlinear optics has also been successfully applied to other 2D materials, such as TMDC systems[208].

Recently, Li et al. combined single-layer continuous transfer, multilayer continuous transfer, and 2D/3D material mixed assembly strategies to construct MoS_2/Al_2O_3 optical crystals with continuously twisted thick layers[57]. As depicted in Figure 8(f), single-crystal monolayer MoS_2 wafers were repeatedly transferred via metal-assisted processes, with alignment angles controlled by wafer-flat edges. Multilayer 3 R-MoS_2 films were then stacked on PDMS surfaces and reassembled into thick-layer crystals through straight-edge alignment, PDMS-assisted transfer, and continuous twist stacking. More importantly, as illustrated in Figure 8(g), optical phase matching was achieved by introducing oxide films and interlayer twist angles in the artificial 3D crystal, resulting in a remarkable 573-fold SHG enhancement.

Taken together, these advances illustrate that both continuous twisting and discrete multilayer stacking approaches are expanding the structural design space of 2D materials. Building on these efforts, an emerging frontier is the deliberate construction of multi-twist-angle or "super-Moiré" structures, in which more than one twist parameter is introduced within a single heterostructure. Unlike conventional bilayer systems defined by a single angle, these architectures provide an expanded design space with multiple Moiré periodicities, yielding richer band reconstructions and unprecedented tunability of correlated states[209,210]. Recent demonstrations include multistep stacking protocols to construct trilayer and multilayer Moiré systems with distinct angles, as well as spiral growth methods that naturally generate rotational gradients across a single flake. In addition, robotic stacking under vacuum has shown promise for integrating multiple layers with sub-degree precision, thereby offering a feasible pathway to controlled multi-angle assemblies.

From a feasibility perspective, the fabrication of super-Moiré structures faces challenges in alignment accuracy, interlayer contamination, and scalability. However, the potential payoffs are substantial: super-Moiré lattices have been predicted and observed to host coexisting flat bands, tunable correlated phases, and topological states[211,212]. These features make them highly relevant not only for fundamental studies of correlated electron systems but also for next-generation optoelectronic and quantum devices. Looking forward, combining the cleanliness of direct growth with the precision of automated stacking may provide viable routes toward large-area super-Moiré fabrication. As such, the development of super-Moiré architectures should be regarded as a critical direction for future research, where advances in fabrication methodology and fundamental physics are expected to reinforce one another.

2.2.4. Vacuum transfer for ultraclean 2D Moiré structure. The clean transfer of 2D materials constitutes a fundamental prerequisite for their reliable characterization and application across diverse scenarios, as it is essential for preserving their intrinsic properties. Conventional transfer techniques, particularly those utilizing metals or 2D materials as transfer media, effectively eliminate organic contamination. However, they inevitably introduce airborne molecular adsorbates at 2D material interfaces. Therefore, vacuum-based transfer strategies offer a powerful solution to this challenge, enabling the assembly of pristine van der Waals interfaces. This principle was demonstrated by Kang et al. who compared the layer-by-layer assembly of multilayer MoS_2 in air versus vacuum[213]. X-ray diffraction characterization revealed that vacuum-stacked samples exhibited a smaller (001) lattice spacing and a reduced full width at half maximum, directly indicating that a cleaner vdW interface was achieved under vacuum. Building upon this foundation, Mannix et al. advanced the methodology by developing a vacuum-based, mechanically controlled system for robotic stacking[46].

Recent breakthroughs have further enhanced ultra-clean transfer capabilities. Shen et al. achieved large-area, ultra-clean transfer of TMDCs under ultra-high vacuum (UHV) 10^{-10} mbar using a metal deposition-assisted dry transfer process, as illustrated in Figure 9(a)[55]. As shown in Figure 9(b), this technique enables the fabrication of novel TMDC/Cu Moiré superlattices, which are unattainable via conventional growth methods due to the redox activity of TMDCs and metals. Critically, this approach creates a conductive metal substrate for TMDCs, which can be used for various subsequent high-fidelity surface-sensitive tests, such as STM and angle-resolved photoemission spectroscopy (ARPES). Figure 9(c) shows that the cleavage chamber of this UHV system is interconnected with various surface testing equipment. The cleanliness afforded by this transfer method, combined with in situ surface-sensitive techniques, allowed the authors to observe a 2×2 charge density wave (CDW) and its Fermi surface nesting mechanism in monolayer MoS_2 for the first time.

In addition to metal deposition-assisted transfer, prefabricated metal films also serve as effective mediators for vacuum-assisted 2D material transfer via a direct lamination approach. Wang et al. used inorganic flexible silicon nitride (SiN_x) films covered with Au films to transfer various 2D materials, thereby fabricating 2D Moiré heterojunctions under UHV conditions[47]. The SiN_x-based transfer layer was fabricated into a cantilever beam structure, the structure and composition of which are shown in Figures 9(d) and (e). As shown in Figure 9(f), the transfer steps are referenced to the metal-assisted transfer in Section 2.2.1. The thickness and composition of the metal film can be changed to adjust the adhesion properties, thereby achieving transfer and release, with a yield of nearly 100% for various 2D materials. The technology is compatible with transfer in air, glove boxes, or

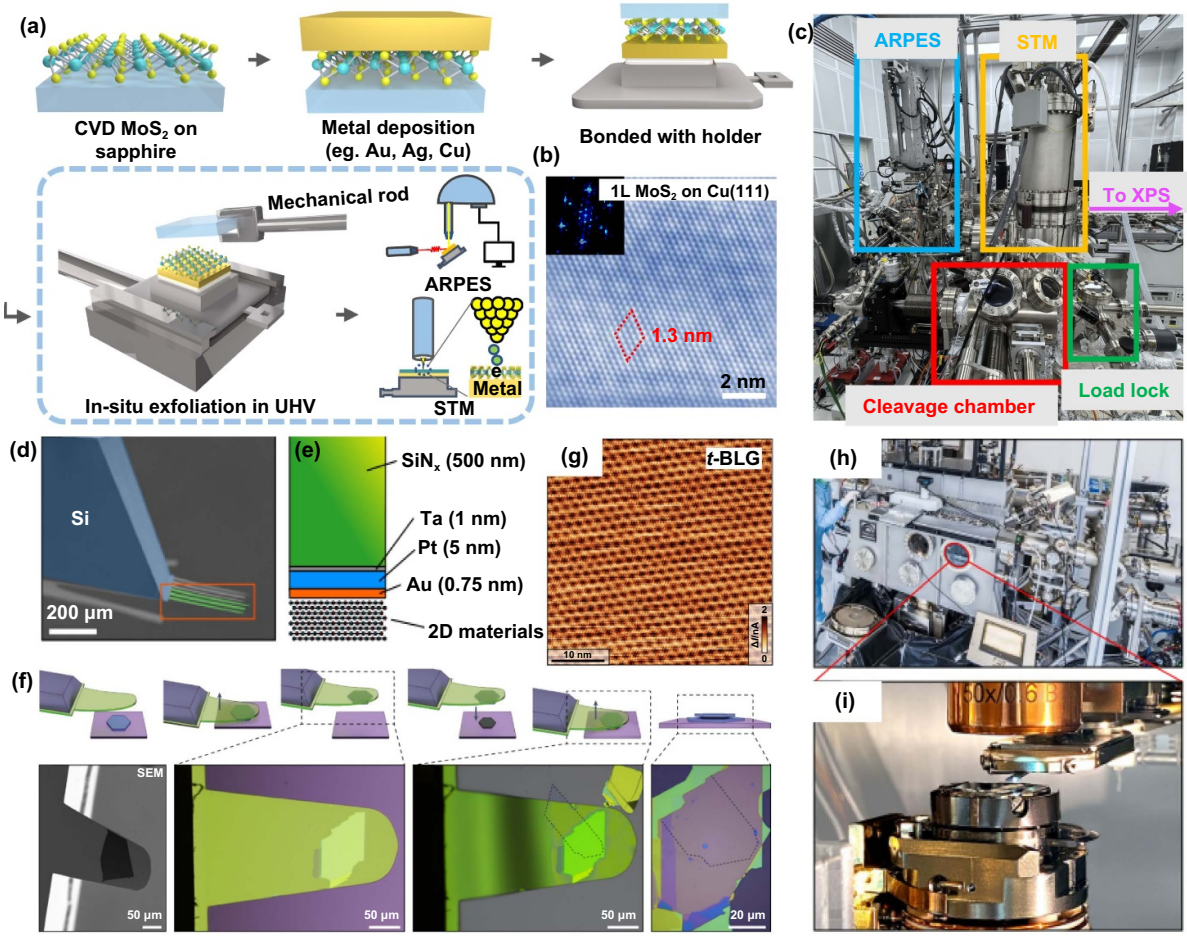

Figure 9. Ultra-high vacuum transfer and assembly of ultraclean 2D Moiré structure. (a) UHV vacuum transfer process of MoS_2 from sapphire to Cu. (b) STM image of the monolayer MoS_2/Cu (111) Moiré heterostructure, the insertion is the corresponding FFT pattern. (c) Picture of the vacuum transfer and characterization chamber. From[55]. Reprinted with permission from AAAS. (d) SEM image of several SiN_x cantilevers protruding from a silicon chip. (e) Schematic image of the multilayer metallic coating of the SiN_x cantilever, holding a 2D material sample. (f) Schematic diagram (top panel) and corresponding photos (bottom panel) of the vacuum assembly process, which involves the picking-up of h-BN and graphene crystal, and finally release on h-BN crystal. (g) c- AFM image of *t*-BLG assembled on h-BN crystal under vacuum. (h) Instrument for performing UHV assembly for 2D material transfer and integration. (i) Close-up of the optical lens, cantilever and sample stage. Reproduced from[47]. CC BY 4.0.

UHV at temperatures up to 350 °C, enabling the reliable fabrication of clean 2D stacks. The twisted graphene heterostructures were assembled in UHV by this technology, and the uniformity of the Moiré superlattice was improved tenfold compared to traditional transfer techniques, as demonstrated by the STM image in Figure 9(g). Figures 9(h) and (i) show the appearance and internal components of this vacuum transfer device, respectively. Vacuum transfer technology has the potential to eliminate the cleanliness bottleneck in the nanofabrication of 2D materials and provide a path to scale up.

2.2.5. In situ dynamic twisting. The transfer and stacking methods enable the flexible construction of artificial Moiré superlattices, accommodating diverse materials and large-scale manufacturing. However, these methods are limited in dynamically controlling the twist angle of the Moiré superlattice. To realize real-time angle regulation, two main approaches—in-situ rotation and in-situ folding—have been developed.

The concept of in-situ rotation originated from the thermally driven rotation observed in 2D materials[43,58,214]. Owing to the ultralow friction between layers of van der Waals materials, twisted flakes can rotate under external forces to minimize the stacking energy[215]. In 2016, Wang et al. demonstrated the directional movement and rotation of graphene on an h-BN surface via AFM tips, dynamically regulating the twist angle and properties of the graphene/h-BN Moiré heterojunction[43]. This strategy has since been applied to other heterojunctions, such as MoS_2/graphene and MoS_2/h-BN[44,58,214]. Figure 10(a) illustrates the AFM-driven movement of MoS_2 domains on graphene[214]. Similarly, in 2018, Palau et al. used AFM tips to control the rotation angle between h-BN and graphene by pushing h-BN as a 'gear,' as shown in Figures 10(b) and (c)[44]. Furthermore, Kapfer et al.

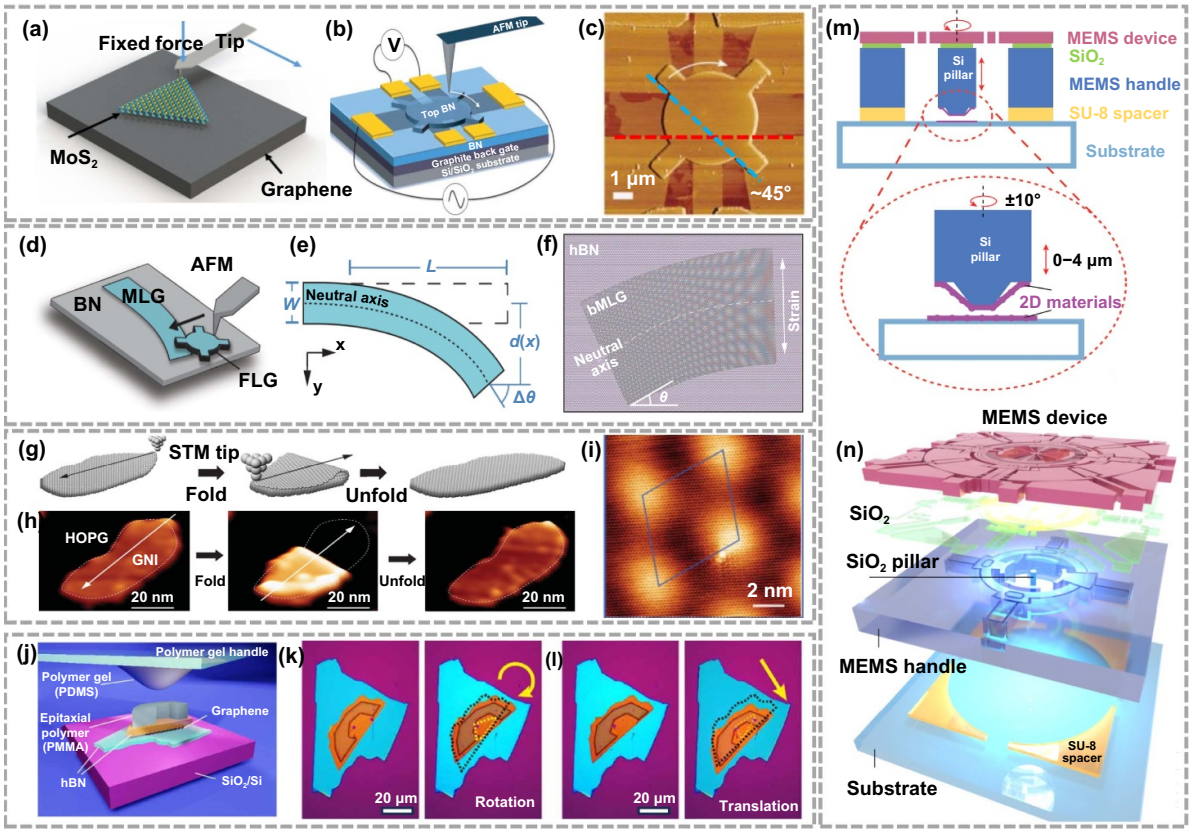

Figure 10. In-situ twisting technology. (a) AFM tip-assisted rotation of MoS_2 on graphene. Reproduced from[215]. CC BY 4.0. (b) and (c) Schematic (b) and AFM image of the AFM tip-assisted rotation of the h-BN gear on graphene. From[44]. Reprinted with permission from AAAS. (d)–(f) In-plane bending of a monolayer 2D ribbon induced by the AFM tip. (e) Relationship between the twist angle and displacement in a 2D bending model. (f) Diagram of a distorted Moiré superlattice, highlighting the effect of strain in the low-angle limit. From[217]. Reprinted with permission from AAAS. (g) and (h) Schematic diagram (g) and STM images (h) of folding and unfolding a GNI by an STM tip. (i) High-resolution STM image of the folded GNI. From[45]. Reprinted with permission from AAAS. (j) Schematic of the polymer-assisted in situ manipulation technique. (k) and (l) Optical images of the stack before (left) and after (right) rotation (k) and translation (l) manipulation. Reproduced from[218]. CC BY 4.0. (m) and (n) Cross-sectional schematic (m) and exploded schematic (n) of the main components in a MEGA2D device. Reproduced from[48], with permission from Springer Nature.

employed AFM tips to manipulate the Moiré patterns of heterogeneous 2D layers by in-plane bending of single-layer 2D ribbons, enabling continuous twist angle variation, as depicted in Figures 10(d)–(f)[216]. This approach offers valuable insights for strain engineering in ultralow-disorder Moiré systems.

In-situ folding is another significant method for creating bilayer structures with adjustable twist angles. The first demonstration of in situ folding was reported by Roy et al. in 1998, who used STM tips to fold and unfold a single graphene layer on a HOPG surface[37]. Later, in 2008, Schniepp et al. achieved reversible folding of graphene sheets using AFM tips to study their bending properties[217]. More recently, in 2019, Chen et al. introduced a precise and versatile technique for graphene origami[45]. As shown in Figures 10(g) and (h), STM manipulation allows graphene nanoislands (GNIs) to fold and unfold along arbitrary directions, forming bilayer graphene with tunable twist angles. Figure 10(i) displays a Moiré pattern of a 1.6° *t*-BLG island obtained through in-situ STM folding.

Both STM- and AFM-driven techniques operate on a microscopic scale, requiring sophisticated equipment and specialized skills. To address these limitations, macro-scale control methods have recently emerged. In 2020, Yang et al. developed a direct in-situ rotation method based on the 'tear-and-stack' technique, enabling dynamic rotation and translation in 2D van der Waals heterostructures[218]. For example, in the PDMS/PMMA/h-BN/graphene/h-BN stack, relative movement between graphene and h-BN is achieved by manipulating the handle layer, thus altering the twist angle, as illustrated in Figures 9(j)–(l). This method has been further advanced with microelectromechanical systems (MEMS) to enable precise, in-situ tuning of 2D interfaces, as shown in Figures 10(m) and (n)[48]. The MEMS-based generic actuation platform for 2D materials (MEGA2D) allows voltage-controlled operations, including approaching, twisting, and pressurizing. A key application of this platform is the development of integrated light sources with real-time, wide-range tunable polarization achieved through dynamic twist angle adjustment. The advancement of in-situ

Table 2. Comparison of major fabrication methods for twisted 2D Moiré.

Fabrication method	Angular precision	Scalability	Interface cleanliness	Device integration suitability
Direct growth	Low (discrete preferred angles)	Moderate	Ultra-clean pristine interface	Limited to substrate-compatible systems
Transfer assembly (manual)	High ($\pm0.1^\circ$–0.5°)	High	Contamination (polymers, residues)	Widely compatible, flexible
Robotic stacking (vacuum)	High ($\pm0.1^\circ$–0.5°)	High	Ultra-clean, vacuum compatible	High, suitable for encapsulated devices
In-situ twisting	Continuous tunability	Lab-scale	Clean	Excellent for fundamental studies

dynamic twistin technology holds significant potential for investigating the structure-property relationship within Moiré superlattices.

2.3. Comparison of major fabrication methods for twisted 2D Moiré

Although a wide variety of fabrication routes for twisted 2D Moiré have been developed, their differences are often more complementary than competitive. To provide a clearer understanding, it is useful to analyze these methods through a comparative framework that highlights their respective advantages, limitations, and application relevance. Table 2 summarizes four major strategies—direct growth, transfer-based assembly, robotic stacking, and in-situ twisting—according to angular precision, scalability, interface cleanliness, and suitability for device integration.

Direct growth methods, including CVD and other epitaxial growth methods, are highly valued for their scalability and pristine interfaces. The absence of polymer residues or external contamination ensures that the resulting heterostructures are ideal for probing intrinsic electronic or optical properties. However, thermodynamic constraints and lattice symmetry strongly bias the stacking orientation, restricting the available twist angles to discrete values. This limitation makes direct growth poorly suited for exploring correlated electron states that demand sub-degree precision, such as the $\sim1.1^\circ$ "magic-angle" in bilayer graphene. Nonetheless, direct growth remains the most practical route for wafer-scale optoelectronic and photonic devices, where large domain size and interface quality outweigh angular flexibility.

In contrast, transfer-based assembly offers a very different balance. Techniques such as polymer-assisted transfer, van der Waals pick-up, or tear-and-stack approaches enable highly accurate angular control, with errors as small as $\pm0.1^\circ$. This makes transfer-based assembly indispensable for fabricating quantum Moiré platforms where flat-band physics, correlated insulating phases, or unconventional superconductivity emerge only within narrow angular windows. However, the reliance on polymer or metal supports inevitably introduces residues, wrinkles, and bubbles, compromising interface cleanliness and reproducibility. As a result, while this route excels in angular precision, its limited scalability and contamination risks hinder large-area device integration.

Robotic stacking under vacuum has recently emerged as a promising strategy for scaling up the fabrication of twisted 2D structures. Compared with manual transfer, robotic platforms provide greater reproducibility, automation, and compatibility with large-area assembly. In particular, vacuum environments suppress interfacial contamination, yielding ultra-clean van der Waals interfaces. A unique advantage of this approach lies in its ability to integrate different types of materials, such as graphene and h-BN, into precisely aligned heterostructures. This multi-material capability makes robotic stacking attractive for optoelectronic and quantum devices requiring encapsulation and dielectric engineering. On the other hand, the technique still faces notable challenges: full automation has so far been optimized for polycrystalline films, while extending to single-crystalline flakes remains difficult, especially when assembling multiple discrete layers. Furthermore, throughput and domain size are constrained by the availability of large-area exfoliated or grown single crystals. Despite these limitations, robotic stacking represents a key intermediate route that balances cleanliness and accuracy with partial scalability, and it is expected to play a central role in bridging laboratory demonstrations and device-level integration.

Finally, in-situ twisting techniques, including AFM manipulation and MEMS-based actuation, provide a unique opportunity to dynamically tune twist angles in real time. This capability allows researchers to continuously explore twist-dependent properties, rather than relying on static, discretely fabricated structures. While such approaches are unlikely to become scalable fabrication routes, they serve as powerful experimental platforms for probing fundamental physics and guiding theoretical models.

Building upon the comparative analysis above, it becomes clear that each fabrication route has distinct advantages but also inherent limitations, and none can simultaneously achieve scalability, angular precision, interface cleanliness, or device compatibility. This realization underscores the need to look beyond conventional bilayer systems and toward emerging architectures with multiple twist angles or "super-Moiré" structures. Unlike single-angle bilayers, these complex assemblies introduce an additional degree of structural

freedom, enabling richer band reconstructions, novel correlated phases, and unprecedented tunability in optical and electronic responses. Recent progress in robotic stacking, spiral growth, and multi-step assembly has demonstrated the feasibility of constructing such multi-angle superlattices. As fabrication techniques evolve, the convergence of precision stacking, ultra-clean transfer, and scalable growth strategies will be critical for translating these proof-of-concept demonstrations into practical platforms. In this context, super-Moiré architectures not only represent a natural extension of current fabrication strategies but also mark a frontier direction where advances in methodology and fundamental physics are likely to reinforce each other, opening new avenues for twistronics research and device innovation.

3. Perspectives

In summary, since the discovery of unconventional superconducting and correlated insulating states in magic-angle *t*-BLG, twisted Moiré superlattices have emerged as a powerful platform for exploring novel properties in 2D materials. Despite significant progress in the fabrication and study of twisted 2D materials over the past two decades, many challenges remain unresolved.

First, in terms of 2D Moiré structure design, substantial advancements have been made in hexagonal Moiré superlattices, but low-symmetry systems have rarely been reported. Symmetry breaking is crucial for tuning the topological electronic states, optoelectronic properties, and electromagnetic polarization of materials. Therefore, developing low-symmetry 2D materials and twisted stacking systems holds immense potential for applications in optical, electrical, and magnetic devices. While some studies have focused on fabricating graphene/BP heterojunctions, there remains a vast space to explore cross-symmetry 2D Moiré systems. Both two-step growth methods and artificial stacking are viable approaches. The construction of such cross-symmetry systems could unlock new avenues for discovering unique properties in 2D materials. Additionally, to achieve more efficient structure-property research, computational efforts should integrate advanced artificial intelligence and big data technologies to predict the unique properties of 2D systems under specific structural configurations and twist angles. This can guide experimental efforts to uncover phenomena akin to the 1.1° magic angle in *t*-BLG.

To controllably construct twisted Moiré superlattices, a direct growth method and artificial stacking strategy have been developed. On the one hand, the direct growth method ensures clean, pristine interfaces but faces three main challenges: (1) the inability to obtain a bilayer structure with a desired twist angle, which is determined by material symmetry and thermodynamic equilibrium. Therefore, breaking the material symmetry or thermodynamic equilibrium during growth is the key to achieving different twist angles. Controlling reaction temperature, temperature gradient, reaction time, and raw material concentration are important factors for managing thermodynamic equilibrium. Changing substrate stress and introducing material defects may alter the material symmetry. (2) The direct growth of twisted heterojunctions remains unreported, which significantly limits progress in this area. However, this field is promising and offers considerable room for exploration. For example, CVD methods used for *t*-BLG and *t*-MoS_2 could be adapted to directly grow twisted TMDC heterojunctions through a two-step process. (3) The lateral dimensions of twisted 2D materials grown via CVD, including *t*-BLG and *t*-MoS_2, are currently limited to less than 10 microns, which restricts their large-scale applications. The 'pre-stacked substrate-angle replication' technology reported by Liu et al. may be further developed to achieve the direct growth of large-area twisted 2D materials other than graphene systems. On the other hand, artificial stacking offers high compatibility but faces challenges of contamination and damage during the stacking process. Compared with wet transfer methods, dry transfer in a high-vacuum environment minimizes contamination from solvents, reduces bubble and wrinkle formation, and prevents damage, making it a promising approach for achieving ultra-clean interfaces. Furthermore, vacuum-compatible techniques enable surface-sensitive analyses, such as scanning electron microscopy and ARPES, allowing for direct observation of the surface electronic states of Moiré superlattices at the atomic scale. Finally, with the development of in-situ dynamic twisting technology, more 'magic angles' and special properties are expected to be discovered in other 2D materials beyond 1.1°-induced superconductivity in *t*-BLG.

Acknowledgments

J S and H C contributed equally to this work. This work was supported by the Westlake Education Foundation.

ORCID iD

Wei Kong 0009-0007-9165-8682

References

[1] Novoselov K S, Geim A K, Morozov S V, Jiang D, Zhang Y, Dubonos S V, Grigorieva I V and Firsov A A. 2004. Electric field effect in atomically thin carbon films. *Science* **306**, 666–669.

[2] Bolotin K I, Sikes K J, Jiang Z, Klima M, Fudenberg G, Hone J, Kim P and Stormer H L. 2008. Ultrahigh electron mobility in suspended graphene. *Solid State Commun.* **146**, 351–355.

[3] Banszerus L, Schmitz M, Engels S, Dauber J, Oellers M, Haupt F, Watanabe K, Taniguchi T, Beschoten B and Stampfer C. 2015. Ultrahigh-mobility graphene devices from chemical vapor deposition on reusable copper. *Sci. Adv.* **1**, e1500222.

[4] Balandin A A, Ghosh S, Bao W Z, Calizo I, Teweldebrhan D, Miao F and Lau C N. 2008. Superior thermal conductivity of single-layer graphene. *Nano Lett.* **8**, 902–907.

[5] Papageorgiou D G, Kinloch I A and Young R J. 2017. Mechanical properties of graphene and graphene-based nanocomposites. *Prog. Mater. Sci.* **90**, 75–127.

[6] Lee C, Wei X D, Kysar J W and Hone J. 2008. Measurement of the elastic properties and intrinsic strength of monolayer graphene. *Science* **321**, 385–388.
[7] Mounet N et al. 2018. Two-dimensional materials from high-throughput computational exfoliation of experimentally known compounds. *Nat. Nanotechnol.* **13**, 246–252.
[8] Shen L, Zhou J, Yang T, Yang M and Feng Y P. 2022. High-throughput computational discovery and intelligent design of two-dimensional functional materials for various applications. *Acc. Mater. Res.* **3**, 572–583.
[9] Zhao B, Shen D Y, Zhang Z C, Lu P, Hossain M, Li J, Li B and Duan X D. 2021. 2D metallic transition-metal dichalcogenides: structures, synthesis, properties, and applications. *Adv. Funct. Mater.* **31**, 2105132.
[10] Son Y W, Cohen M L and Louie S G. 2006. Half-metallic graphene nanoribbons. *Nature* **444**, 347–349.
[11] Liu H, Du Y C, Deng Y X and Ye P D. 2015. Semiconducting black phosphorus: synthesis, transport properties and electronic applications. *Chem. Soc. Rev.* **44**, 2732–2743.
[12] Su S K, Chuu C P, Li M Y, Cheng C C, Wong H S P and Li L J. 2021. Layered semiconducting 2D materials for future transistor applications. *Small Struct.* **2**, 2000103.
[13] Song L et al. 2010. Large scale growth and characterization of atomic hexagonal boron nitride layers. *Nano Lett.* **10**, 3209–3215.
[14] Illarionov Y Y et al. 2020. Insulators for 2D nanoelectronics: the gap to bridge. *Nat. Commun.* **11**, 3385.
[15] Akinwande D, Huyghebaert C, Wang C H, Serna M I, Goossens S, Li L J, Wong H S P and Koppens F H L. 2019. Graphene and two-dimensional materials for silicon technology. *Nature* **573**, 507–518.
[16] Chhowalla M, Jena D and Zhang H. 2016. Two-dimensional semiconductors for transistors. *Nat. Rev. Mater.* **1**, 16052.
[17] Zhou X, Hu X Z, Yu J, Liu S Y, Shu Z W, Zhang Q, Li H Q, Ma Y, Xu H and Zhai T Y. 2018. 2D layered material-based van der Waals heterostructures for optoelectronics. *Adv. Funct. Mater.* **28**, 1706587.
[18] Wang Q H, Kalantar-Zadeh K, Kis A, Coleman J N and Strano M S. 2012. Electronics and optoelectronics of two-dimensional transition metal dichalcogenides. *Nat. Nanotechnol.* **7**, 699–712.
[19] Andrei E Y and MacDonald A H. 2020. Graphene bilayers with a twist. *Nat. Mater.* **19**, 1265–1275.
[20] Carr S, Fang S A and Kaxiras E. 2020. Electronic-structure methods for twisted moiré layers. *Nat. Rev. Mater.* **5**, 748–763.
[21] Xiao Y, Liu J L and Fu L. 2020. Moiré is more: access to new properties of two-dimensional layered materials. *Matter* **3**, 1142–1161.
[22] Andrei E Y, Efetov D K, Jarillo-Herrero P, MacDonald A H, Mak K F, Senthil T, Tutuc E, Yazdani A and Young A F. 2021. The marvels of moiré materials. *Nat. Rev. Mater.* **6**, 201–206.
[23] Cao Y, Fatemi V, Fang S A, Watanabe K, Taniguchi T, Kaxiras E and Jarillo-Herrero P. 2018. Unconventional superconductivity in magic-angle graphene superlattices. *Nature* **556**, 43–50.
[24] Cai L and Yu G. 2021. Fabrication strategies of twisted bilayer graphenes and their unique properties. *Adv. Mater.* **33**, 2004974.
[25] Cheng Y, Huang C, Hong H, Zhao Z X and Liu K H. 2019. Emerging properties of two-dimensional twisted bilayer materials. *Chin. Phys. B* **28**, 107304.
[26] Albrecht T R, Mizes H A, Nogami J, Park S I and Quate C F. 1988. Observation of tilt boundaries in graphite by scanning tunneling microscopy and associated multiple tip effects. *Appl. Phys. Lett.* **52**, 362–364.
[27] Hass J, Varchon F, Millán-Otoya J E, Sprinkle M, Sharma N, de Heer W A, Berger C, First P N, Magaud L and Conrad E H. 2008. Why multilayer graphene on 4*H* SiC (000 1^{-}) Behaveslike a single sheet of graphene. *Phys. Rev. Lett.* **100**, 125504.
[28] Havener R W, Zhuang H L, Brown L, Hennig R G and Park J. 2012. Angle-resolved Raman imaging of interlayer rotations and interactions in twisted bilayer graphene. *Nano Lett.* **12**, 3162–3167.
[29] Fallahazad B, Hao Y F, Lee K, Kim S, Ruoff R S and Tutuc E. 2012. Quantum hall effect in Bernal stacked and twisted bilayer graphene grown on Cu by chemical vapor deposition. *Phys. Rev. B* **85**, 201408.
[30] Brown L, Hovden R, Huang P S E, Wojcik M, Muller D A and Park J. 2012. Twinning and twisting of tri- and bilayer graphene. *Nano Lett.* **12**, 1609–1615.
[31] Sun L Z et al. 2021. Hetero-site nucleation for growing twisted bilayer graphene with a wide range of twist angles. *Nat. Commun.* **12**, 2391.
[32] Liu S et al. 2024. In situ growth of high-quality single-crystal twisted bilayer graphene on liquid copper. *Adv. Mater.* **36**, 2312125.
[33] Xu M Z et al. 2024. Reconfiguring nucleation for CVD growth of twisted bilayer MoS_2 with a wide range of twist angles. *Nat. Commun.* **15**, 562.
[34] Zhou J et al. 2024. Homo-site nucleation growth of twisted bilayer MoS_2 with commensurate angles. *Adv. Mater.* **36**, 2408227.
[35] Liu C et al. 2022. Designed growth of large bilayer graphene with arbitrary twist angles. *Nat. Mater.* **21**, 1263–1268.
[36] Hiura H, Ebbesen T W, Fujita J, Tanigaki K and Takada T. 1994. Role of sp^3 defect structures in graphite and carbon nanotubes. *Nature* **367**, 148–151.
[37] Roy H V, Kallinger C, Marsen B and Sattler K. 1998. Manipulation of graphitic sheets using a tunneling microscope. *J. Appl. Phys.* **83**, 4695–4699.
[38] Ni Z H, Wang Y Y, Yu T, You Y M and Shen Z X. 2008. Reduction of Fermi velocity in folded graphene observed by resonance Raman spectroscopy. *Phys. Rev. B* **77**, 235403.
[39] Kim K, Coh S, Tan L Z, Regan W, Yuk J M, Chatterjee E, Crommie M F, Cohen M L, Louie S G and Zettl A. 2012. Raman spectroscopy study of rotated double-layer graphene: misorientation-angle dependence of electronic structure. *Phys. Rev. Lett.* **108**, 246103.
[40] Chen X D, Xin W, Jiang W S, Liu Z B, Chen Y S and Tian J G. 2016. High-precision twist-controlled bilayer and trilayer graphene. *Adv. Mater.* **28**, 2563–2570.
[41] Kim K et al. 2016. van der Waals heterostructures with high accuracy rotational alignment. *Nano Lett.* **16**, 1989–1995.
[42] Kim C J, Sánchez-Castillo A, Ziegler Z, Ogawa Y, Noguez C and Park J. 2016. Chiral atomically thin films. *Nat. Nanotechnol.* **11**, 520–524.
[43] Wang D M et al. 2016. Thermally induced graphene rotation on hexagonal boron nitride. *Phys. Rev. Lett.* **116**, 126101.
[44] Ribeiro-Palau R, Zhang C J, Watanabe K, Taniguchi T, Hone J and Dean C R. 2018. Twistable electronics with dynamically rotatable heterostructures. *Science* **361**, 690–693.
[45] Chen H et al. 2019. Atomically precise, custom-design origami graphene nanostructures. *Science* **365**, 1036–1040.
[46] Mannix A J et al. 2022. Robotic four-dimensional pixel assembly of van der Waals solids. *Nat. Nanotechnol.* **17**, 361–366.
[47] Wang W D et al. 2023. Clean assembly of van der Waals heterostructures using silicon nitride membranes. *Nat. Electron.* **6**, 981–990.
[48] Tang H N, Wang Y T, Ni X Q, Watanabe K, Taniguchi T, Jarillo-Herrero P, Fan S H, Mazur E, Yacoby A and Cao Y. 2024. On-chip multi-degree-of-freedom control of two-dimensional materials. *Nature* **632**, 1038–1044.

[49] Rong Z Y and Kuiper P. 1993. Electronic effects in scanning tunneling microscopy: moiré pattern on a graphite surface. *Phys. Rev. B* **48**, 17427–17431.
[50] Li L X, Liu R P, Chen Z W, Wang Q, Ma M Z, Jing Q, Li G and Tian Y. 2006. Tearing, folding and deformation of a carbon–carbon sp^2-bonded network. *Carbon* **44**, 1544–1547.
[51] Carozo V, Almeida C M, Ferreira E H M, Cançado L G, Achete C A and Jorio A. 2011. Raman signature of graphene superlattices. *Nano Lett.* **11**, 4527–4534.
[52] Carozo V et al. 2013. Resonance effects on the Raman spectra of graphene superlattices. *Phys. Rev. B* **88**, 085401.
[53] Ni Z H, Liu L, Wang Y Y, Zheng Z, Li L J, Yu T and Shen Z X. 2009. *G*-band Raman double resonance in twisted bilayer graphene: evidence of band splitting and folding. *Phys. Rev. B* **80**, 125404.
[54] Wang Y Y, Ni Z H, Liu L, Liu Y H, Cong C X, Yu T, Wang X J, Shen D Z and Shen Z X. 2010. Stacking-dependent optical conductivity of bilayer graphene. *ACS Nano* **4**, 4074–4080.
[55] Shen J C et al. 2025. Metal-assisted vacuum transfer enabling in situ visualization of charge density waves in monolayer MoS_2. *Sci. Adv.* **11**, eadr9753.
[56] Shen J C, Zhu H Z, Sun X C, Chen H, Ji C, Li W H and Kong W. 2025. Van der Waals assembly of multilayer twisted transition metal dichalcogenides with controllable chirality. *Adv. Funct. Mater.* **35**, 2504859.
[57] Li W H et al. 2025. 3D crystal construction by single-crystal 2D material supercell multiplying. *Adv. Sci.* **12**, 2411656.
[58] Yu H et al. 2017. Precisely aligned monolayer MoS_2 epitaxially grown on h-BN basal plane. *Small* **13**, 1603005.
[59] Wang S X, Cui X H, Jian C E, Cheng H W, Niu M M, Yu J, Yan J X and Huang W. 2021. Stacking-engineered heterostructures in transition metal dichalcogenides. *Adv. Mater.* **33**, 2005735.
[60] Guo H W, Hu Z, Liu Z B and Tian J G. 2021. Stacking of 2D materials. *Adv. Funct. Mater.* **31**, 2007810.
[61] Gao X G, Li X K, Xin W, Chen X D, Liu Z B and Tian J G. 2020. Fabrication, optical properties, and applications of twisted two-dimensional materials. *Nanophotonics* **9**, 1717–1742.
[62] Xin K Y, Wang X G, Grove-Rasmussen K and Wei Z M. 2022. Twist-angle two-dimensional superlattices and their application in (opto)electronics. *J. Semicond.* **43**, 011001.
[63] Hennighausen Z and Kar S. 2021. Twistronics: a turning point in 2D quantum materials. *Electron. Struct.* **3**, 014004.
[64] Schranghamer T F, Sharma M, Singh R and Das S. 2021. Review and comparison of layer transfer methods for two-dimensional materials for emerging applications. *Chem. Soc. Rev.* **50**, 11032–11054.
[65] Cao C H, Wu T Y and Sun Y. 2021. A review of assembly techniques for fabricating twisted bilayer graphene. *J. Micromech. Microeng.* **31**, 114004.
[66] Onodera M, Masubuchi S, Moriya R and Machida T. 2020. Assembly of van der Waals heterostructures: exfoliation, searching, and stacking of 2D materials. *Jpn. J. Appl. Phys.* **59**, 010101.
[67] Tarnopolsky G, Kruchkov A J and Vishwanath A. 2019. Origin of magic angles in twisted bilayer graphene. *Phys. Rev. Lett.* **122**, 106405.
[68] Lisi S et al. 2021. Observation of flat bands in twisted bilayer graphene. *Nat. Phys.* **17**, 189–193.
[69] Shabani S, Halbertal D, Wu W J, Chen M X, Liu S, Hone J, Yao W, Basov D N, Zhu X Y and Pasupathy A N. 2021. Deep moiré potentials in twisted transition metal dichalcogenide bilayers. *Nat. Phys.* **17**, 720–725.
[70] Andersen T I et al. 2021. Excitons in a reconstructed moiré potential in twisted WSe_2/WSe_2 homobilayers. *Nat. Mater.* **20**, 480–487.
[71] Nayak P K et al. 2017. Probing evolution of twist-angle-dependent interlayer excitons in $MoSe_2/WSe_2$ van der Waals heterostructures. *ACS Nano* **11**, 4041–4050.
[72] Jin C H et al. 2019. Observation of moiré excitons in WSe_2/WS_2 heterostructure superlattices. *Nature* **567**, 76–80.
[73] Du L J, Hasan T, Castellanos-Gomez A, Liu G B, Yao Y G, Lau C N and Sun Z P. 2021. Engineering symmetry breaking in 2D layered materials. *Nat. Rev. Phys.* **3**, 193–206.
[74] Xu Y J, Shi Z, Shi X Y, Zhang K and Zhang H. 2019. Recent progress in black phosphorus and black-phosphorus-analogue materials: properties, synthesis and applications. *Nanoscale* **11**, 14491–14527.
[75] Scanlon D O, Watson G W, Payne D J, Atkinson G R, Egdell R G and Law D S L. 2010. Theoretical and experimental study of the electronic structures of MoO_3 and MoO_2. *J. Phys. Chem. C* **114**, 4636–4645.
[76] Zhang T L et al. 2019. Magnetism and optical anisotropy in van der Waals antiferromagnetic insulator CrOCl. *ACS Nano* **13**, 11353–11362.
[77] Cao Y et al. 2018. Correlated insulator behaviour at half-filling in magic-angle graphene superlattices. *Nature* **556**, 80–84.
[78] Wang H F, Ma S J, Zhang S and Lei D Y. 2022. Intrinsic superflat bands in general twisted bilayer systems. *Light Sci. Appl.* **11**, 159.
[79] Zhang L et al. 2020. Twist-angle dependence of moiré excitons in $WS_2/MoSe_2$ heterobilayers. *Nat. Commun.* **11**, 5888.
[80] Weston A et al. 2020. Atomic reconstruction in twisted bilayers of transition metal dichalcogenides. *Nat. Nanotechnol.* **15**, 592–597.
[81] Tran K et al. 2019. Evidence for moiré excitons in van der Waals heterostructures. *Nature* **567**, 71–75.
[82] Bao H W, Miao Y P, Li Y, Bai H Z and Ma F. 2022. Unveiling the moiré pattern evolution and superlubricity in twisted bilayer 2D phosphorene at atomistic scale. *Appl. Surf. Sci.* **606**, 154796.
[83] Liu Y P et al. 2018. Tailoring sample-wide pseudo-magnetic fields on a graphene-black phosphorus heterostructure. *Nat. Nanotechnol.* **13**, 828–834.
[84] Zhao S L et al. 2021. Anisotropic moiré optical transitions in twisted monolayer/bilayer phosphorene heterostructures. *Nat. Commun.* **12**, 3947.
[85] Kang P, Zhang W T, Michaud-Rioux V, Wang X, Yun J N and Guo H. 2020. Twistronics in tensile strained bilayer black phosphorus. *Nanoscale* **12**, 12909–12916.
[86] Wu M H, Qian X F and Li J. 2014. Tunable exciton funnel using moiré superlattice in twisted van der Waals bilayer. *Nano Lett.* **14**, 5350–5357.
[87] Pan D X, Wang T C, Xiao W D, Hu D M and Yao Y G. 2017. Simulations of twisted bilayer orthorhombic black phosphorus. *Phys. Rev. B* **96**, 041411(R).
[88] Hermann K. 2012. Periodic overlayers and moiré patterns: theoretical studies of geometric properties. *J. Phys.: Condens. Matter* **24**, 314210.
[89] Trambly de Laissardière G, Mayou D and Magaud L. 2010. Localization of Dirac electrons in rotated graphene bilayers. *Nano Lett.* **10**, 804–808.
[90] Yankowitz M, Xue J M, Cormode D, Sanchez-Yamagishi J D, Watanabe K, Taniguchi T, Jarillo-Herrero P, Jacquod P and LeRoy B J. 2012. Emergence of superlattice Dirac points in graphene on hexagonal boron nitride. *Nat. Phys.* **8**, 382–386.
[91] Mak K F and Shan J. 2022. Semiconductor Moiré materials. *Nat. Nanotechnol.* **17**, 686–695.
[92] Qian K et al. 2020. Air-stable monolayer Cu_2Se exhibits a purely thermal structural phase transition. *Adv. Mater.* **32**, 1908314.

[93] Akamatsu T et al. 2021. A van der Waals interface that creates in-plane polarization and a spontaneous photovoltaic effect. *Science* **372**, 68–72.
[94] Zheng X M et al. 2022. Symmetry engineering induced in-plane polarization in MoS_2 through van der Waals interlayer coupling. *Adv. Funct. Mater.* **32**, 2202658.
[95] Uchida K, Furuya S, Iwata J I and Oshiyama A. 2014. Atomic corrugation and electron localization due to Moiré patterns in twisted bilayer graphenes. *Phys. Rev. B* **90**, 155451.
[96] Bistritzer R and MacDonald A H. 2011. Moiré bands in twisted double-layer graphene. *Proc. Natl Acad. Sci. USA* **108**, 12233–12237.
[97] San-Jose P, González J and Guinea F. 2012. Non-Abelian gauge potentials in graphene bilayers. *Phys. Rev. Lett.* **108**, 216802.
[98] Yoo H et al. 2019. Atomic and electronic reconstruction at the van der Waals interface in twisted bilayer graphene. *Nat. Mater.* **18**, 448–453.
[99] Lopes Dos Santos J M B, Peres N M R and Castro Neto A H. 2007. Graphene bilayer with a twist: electronic structure. *Phys. Rev. Lett.* **99**, 256802.
[100] Li G H, Luican A, Lopes Dos Santos J M B, Castro Neto A H, Reina A, Kong J and Andrei E Y. 2010. Observation of van Hove singularities in twisted graphene layers. *Nat. Phys.* **6**, 109–113.
[101] Brihuega I, Mallet P, González-Herrero H, Trambly de Laissardière G, Ugeda M M, Magaud L, Gómez-Rodríguez J M, Ynduráin F and Veuillen J Y. 2012. Unraveling the intrinsic and robust nature of van Hove singularities in twisted bilayer graphene by scanning tunneling microscopy and theoretical analysis. *Phys. Rev. Lett.* **109**, 196802.
[102] Latil S, Meunier V and Henrard L. 2007. Massless fermions in multilayer graphitic systems with misoriented layers: *ab initio* calculations and experimental fingerprints. *Phys. Rev. B* **76**, 201402.
[103] Shallcross S, Sharma S and Pankratov O A. 2008. Quantum interference at the twist boundary in graphene. *Phys. Rev. Lett.* **101**, 056803.
[104] Ramasubramaniam A, Naveh D and Towe E. 2011. Tunable band gaps in bilayer graphene−BN heterostructures. *Nano Lett.* **11**, 1070–1075.
[105] Lu X B et al. 2021. Multiple flat bands and topological Hofstadter butterfly in twisted bilayer graphene close to the second magic angle. *Proc. Natl Acad. Sci. USA* **118**, e2100006118.
[106] Otteneder M, Hubmann S, Lu X B, Kozlov D A, Golub L E, Watanabe K, Taniguchi T, Efetov D K and Ganichev S D. 2020. Terahertz photogalvanics in twisted bilayer graphene close to the second magic angle. *Nano Lett.* **20**, 7152–7158.
[107] Arora H S et al. 2020. Superconductivity in metallic twisted bilayer graphene stabilized by WSe_2. *Nature* **583**, 379–384.
[108] Codecido E et al. 2019. Correlated insulating and superconducting states in twisted bilayer graphene below the magic angle. *Sci. Adv.* **5**, eaaw9770.
[109] Vahedi J, Peters R, Missaoui A, Honecker A and Trambly de Laissardière G. 2021. Magnetism of magic-angle twisted bilayer graphene. *SciPost Phys.* **11**, 083.
[110] Rozen A et al. 2021. Entropic evidence for a Pomeranchuk effect in magic-angle graphene. *Nature* **592**, 214–219.
[111] de Vries F K, Portolés E, Zheng G, Taniguchi T, Watanabe K, Ihn T, Ensslin K and Rickhaus P. 2021. Gate-defined Josephson junctions in magic-angle twisted bilayer graphene. *Nat. Nanotechnol.* **16**, 760–763.
[112] Serlin M, Tschirhart C L, Polshyn H, Zhang Y, Zhu J, Watanabe K, Taniguchi T, Balents L and Young A F. 2020. Intrinsic quantized anomalous Hall effect in a moiré heterostructure. *Science* **367**, 900–903.
[113] Yankowitz M, Chen S W, Polshyn H, Zhang Y X, Watanabe K, Taniguchi T, Graf D, Young A F and Dean C R. 2019. Tuning superconductivity in twisted bilayer graphene. *Science* **363**, 1059–1064.
[114] Li S Y, Zhang Y, Ren Y N, Liu J P, Dai X and He L. 2020. Experimental evidence for orbital magnetic moments generated by moiré-scale current loops in twisted bilayer graphene. *Phys. Rev. B* **102**, 121406.
[115] Deng B C, Ma C, Wang Q Y, Yuan S F, Watanabe K, Taniguchi T, Zhang F and Xia F N. 2020. Strong mid-infrared photoresponse in small-twist-angle bilayer graphene. *Nat. Photon.* **14**, 549–553.
[116] Kim Y, Moon P, Watanabe K, Taniguchi T and Smet J H. 2021. Odd integer quantum Hall states with interlayer coherence in twisted bilayer graphene. *Nano Lett.* **21**, 4249–4254.
[117] Yin J B et al. 2016. Selectively enhanced photocurrent generation in twisted bilayer graphene with van Hove singularity. *Nat. Commun.* **7**, 10699.
[118] Ahn S J et al. 2018. Dirac electrons in a dodecagonal graphene quasicrystal. *Science* **361**, 782–786.
[119] Yasuda K, Wang X R, Watanabe K, Taniguchi T and Jarillo-Herrero P. 2021. Stacking-engineered ferroelectricity in bilayer boron nitride. *Science* **372**, 1458–1462.
[120] Kim H, Leconte N, Chittari B L, Watanabe K, Taniguchi T, MacDonald A H, Jung J and Jung S. 2018. Accurate gap determination in monolayer and bilayer graphene/*h*-BN moiré superlattices. *Nano Lett.* **18**, 7732–7741.
[121] Jung J, DaSilva A M, MacDonald A H and Adam S. 2015. Origin of band gaps in graphene on hexagonal boron nitride. *Nat. Commun.* **6**, 6308.
[122] Hunt B et al. 2013. Massive Dirac fermions and Hofstadter butterfly in a van der Waals heterostructure. *Science* **340**, 1427–1430.
[123] Gorbachev R V et al. 2014. Detecting topological currents in graphene superlattices. *Science* **346**, 448–451.
[124] Wang T L, Bultinck N and Zaletel M P. 2020. Flat-band topology of magic angle graphene on a transition metal dichalcogenide. *Phys. Rev. B* **102**, 235146.
[125] Özçelik V O, Azadani J G, Yang C, Koester S J and Low T. 2016. Band alignment of two-dimensional semiconductors for designing heterostructures with momentum space matching. *Phys. Rev. B* **94**, 035125.
[126] Wakamura T, Reale F, Palczynski P, Zhao M Q, Johnson A T C, Guéron S, Mattevi C, Ouerghi A and Bouchiat H. 2019. Spin-orbit interaction induced in graphene by transition metal dichalcogenides. *Phys. Rev. B* **99**, 245402.
[127] Wu F C, Lovorn T, Tutuc E, Martin I and MacDonald A H. 2019. Topological insulators in twisted transition metal dichalcogenide homobilayers. *Phys. Rev. Lett.* **122**, 086402.
[128] Wang L et al. 2020. Correlated electronic phases in twisted bilayer transition metal dichalcogenides. *Nat. Mater.* **19**, 861–866.
[129] Li T X et al. 2021. Quantum anomalous Hall effect from intertwined moiré bands. *Nature* **600**, 641–646.
[130] Zhang Y, Devakul T and Fu L. 2021. Spin-textured Chern bands in AB-stacked transition metal dichalcogenide bilayers. *Proc. Natl Acad. Sci. USA* **118**, e2112673118.
[131] Wang X R, Yasuda K, Zhang Y, Liu S, Watanabe K, Taniguchi T, Hone J, Fu L and Jarillo-Herrero P. 2022. Interfacial ferroelectricity in rhombohedral-stacked bilayer transition metal dichalcogenides. *Nat. Nanotechnol.* **17**, 367–371.
[132] Wang X et al. 2022. Light-induced ferromagnetism in moiré superlattices. *Nature* **604**, 468–473.
[133] Rosenberger M R, Chuang H J, Phillips M, Oleshko V P, McCreary K M, Sivaram S V, Hellberg C S and Jonker B T. 2020. Twist angle-dependent atomic reconstruction and Moire´ patterns in transition metal dichalcogenide heterostructures. *ACS Nano* **14**, 4550–4558.

[134] Wang P J et al. 2022. One-dimensional Luttinger liquids in a two-dimensional moiré lattice. *Nature* **605**, 57–62.
[135] Fang T, Liu T R, Jiang Z N, Yang R, Servati P and Xia G R. 2019. Fabrication and the interlayer coupling effect of twisted stacked black phosphorus for optical applications. *ACS Appl. Nano Mater.* **2**, 3138–3145.
[136] Srivastava P K et al. 2021. Resonant tunnelling diodes based on twisted black phosphorus homostructures. *Nat. Electron.* **4**, 269–276.
[137] Kang P, Zhang W T, Michaud-Rioux V, Kong X H, Hu C, Yu G H and Guo H. 2017. Moiré impurities in twisted bilayer black phosphorus: effects on the carrier mobility. *Phys. Rev. B* **96**, 195406.
[138] Chen M Y, Lin X, Dinh T H, Zheng Z R, Shen J L, Ma Q, Chen H S, Jarillo-Herrero P and Dai S Y. 2020. Configurable phonon polaritons in twisted α-MoO_3. *Nat. Mater.* **19**, 1307–1311.
[139] Gou J, Kong L J, He X Y, Huang Y L, Sun J T, Meng S, Wu K H, Chen L and Wee A T S. 2020. The effect of moiré superstructures on topological edge states in twisted bismuthene homojunctions. *Sci. Adv.* **6**, eaba2773.
[140] Liu Y W, Qiao J B, Yan C, Zhang Y, Li S Y and He L. 2019. Magnetism near half-filling of a van Hove singularity in twisted graphene bilayer. *Phys. Rev. B* **99**, 201408.
[141] Kurebayashi H, Garcia J H, Khan S, Sinova J and Roche S. 2022. Magnetism, symmetry and spin transport in van der Waals layered systems. *Nat. Rev. Phys.* **4**, 150–166.
[142] Thomson A, Chatterjee S, Sachdev S and Scheurer M S. 2018. Triangular antiferromagnetism on the honeycomb lattice of twisted bilayer graphene. *Phys. Rev. B* **98**, 075109.
[143] Saito Y, Ge J Y, Rademaker L, Watanabe K, Taniguchi T, Abanin D A and Young A F. 2021. Hofstadter subband ferromagnetism and symmetry-broken Chern insulators in twisted bilayer graphene. *Nat. Phys.* **17**, 478–481.
[144] Nuckolls K P, Oh M, Wong D, Lian B, Watanabe K, Taniguchi T, Bernevig B A and Yazdani A. 2020. Strongly correlated Chern insulators in magic-angle twisted bilayer graphene. *Nature* **588**, 610–615.
[145] Wu S, Zhang Z Y, Watanabe K, Taniguchi T and Andrei E Y. 2021. Chern insulators, van Hove singularities and topological flat bands in magic-angle twisted bilayer graphene. *Nat. Mater.* **20**, 488–494.
[146] Chhowalla M, Shin H S, Eda G, Li L J, Loh K P and Zhang H. 2013. The chemistry of two-dimensional layered transition metal dichalcogenide nanosheets. *Nat. Chem.* **5**, 263–275.
[147] Choi W, Choudhary N, Han G H, Park J, Akinwande D and Lee Y H. 2017. Recent development of two-dimensional transition metal dichalcogenides and their applications. *Mater. Today* **20**, 116–130.
[148] Manzeli S, Ovchinnikov D, Pasquier D, Yazyev O V and Kis A. 2017. 2D transition metal dichalcogenides. *Nat. Rev. Mater.* **2**, 17033.
[149] Hass J, de Heer W A and Conrad E H. 2008. The growth and morphology of epitaxial multilayer graphene. *J. Phys.: Condens. Matter* **20**, 323202.
[150] Miller D L, Kubista K D, Rutter G M, Ruan M, de Heer W A, First P N and Stroscio J A. 2010. Structural analysis of multilayer graphene via atomic moiré interferometry. *Phys. Rev. B* **81**, 125427.
[151] Yan Z et al. 2014. Large hexagonal bi- and trilayer graphene single crystals with varied interlayer rotations. *Angew. Chem., Int. Ed.* **53**, 1565–1569.
[152] Lu C C, Lin Y C, Liu Z, Yeh C H, Suenaga K and Chiu P W. 2013. Twisting bilayer graphene superlattices. *ACS Nano* **7**, 2587–2594.
[153] Dong J C, Zhang L N and Ding F. 2019. Kinetics of graphene and 2D materials growth. *Adv. Mater.* **31**, 1801583.
[154] Cai Z Y, Liu B L, Zou X L and Cheng H M. 2018. Chemical vapor deposition growth and applications of two-dimensional materials and their heterostructures. *Chem. Rev.* **118**, 6091–6133.
[155] Liu C, Wang L, Qi J J and Liu K H. 2020. Designed growth of large-size 2D single crystals. *Adv. Mater.* **32**, 2000046.
[156] Tang L, Tan J Y, Nong H Y, Liu B L and Cheng H M. 2020. Chemical vapor deposition growth of two-dimensional compound materials: controllability, material quality, and growth mechanism. *Acc. Mater. Res.* **2**, 36–47.
[157] Zhang L N, Dong J C and Ding F. 2021. Strategies, status, and challenges in wafer scale single crystalline two-dimensional materials synthesis. *Chem. Rev.* **121**, 6321–6372.
[158] Song X J et al. 2016. Seed-assisted growth of single-crystalline patterned graphene domains on hexagonal boron nitride by chemical vapor deposition. *Nano Lett.* **16**, 6109–6116.
[159] Ago H, Endo H, Solís-Fernández P, Takizawa R, Ohta Y, Fujita Y, Yamamoto K and Tsuji M. 2015. Controlled van der Waals epitaxy of monolayer MoS_2 triangular domains on graphene. *ACS Appl. Mater. Interfaces* **7**, 5265–5273.
[160] Okada M, Sawazaki T, Watanabe K, Taniguch T, Hibino H, Shinohara H and Kitaura R. 2014. Direct chemical vapor deposition growth of WS_2 atomic layers on hexagonal boron nitride. *ACS Nano* **8**, 8273–8277.
[161] Fu Q D et al. 2018. One-step synthesis of metal/semiconductor heterostructure NbS_2/MoS_2. *Chem. Mater.* **30**, 4001–4007.
[162] Liu P F, Feng L P, Zhang X D, Yang Y L, Zheng X Q and Wang X T. 2024. Bottom-up growth of high-quality BiOCl twisted homostructures via a precursor regulation strategy. *Mater. Today* **80**, 40–49.
[163] Liu K H, Zhang L, Cao T, Jin C, Qiu D, Zhou Q, Zettl A, Yang P, Louie S G and Wang F. 2014. Evolution of interlayer coupling in twisted molybdenum disulfide bilayers. *Nat. Commun.* **5**, 4966.
[164] Wang Q, Wang X C, Lou Q W, Jiang Y and Fan X P. 2024. Two-dimensional spiral: a promising Moiré superlattice. *Laser Photon. Rev.* **19**, 2401368.
[165] Wang Z-J et al. 2024. Conversion of chirality to twisting via sequential one-dimensional and two-dimensional growth of graphene spirals. *Nat. Mater.* **23**, 331–338.
[166] Zhao Y Z and Jin S. 2022. Stacking and twisting of layered materials enabled by screw dislocations and non-Euclidean surfaces. *Acc. Mater. Res.* **3**, 369–378.
[167] Peng J B, Ren C X, Zhang W L, Chen H, Pan X G, Bai H X, Jing F L, Qiu H L, Liu H J and Hu Z G. 2022. Spatially dependent electronic structures and excitons in a marginally twisted Moiré superlattice of spiral WS_2. *ACS Nano* **16**, 21600–21608.
[168] Zhao Y Z, Zhang C Y, Kohler D D, Scheeler J M, Wright J C, Voyles P M and Jin S. 2020. Supertwisted spirals of layered materials enabled by growth on non-Euclidean surfaces. *Science* **370**, 442–445.
[169] Tong T et al. 2024. Giant second harmonic generation in supertwisted WS_2 spirals grown in step-edge particle-induced non-Euclidean surfaces. *ACS Nano* **18**, 21939–21947.
[170] Chen J Y, Bai Y, Qi M, Zhang W X, Qin C B, Fan X P and Xiao L T. 2025. Structure-dependent nonlinear optical effects in spiral WS_2 nanosheets. *Adv. Mater.* **37**, 2415214.
[171] Su M X, Zhou W D, Liu L, Chen M Y, Jiang Z Z, Luo X F, Yang Y, Yu T, Lei W and Yuan C L. 2022. Micro eddy current facilitated by screwed MoS_2 structure for enhanced hydrogen evolution reaction. *Adv. Funct. Mater.* **32**, 2111067.
[172] Wang X Z et al. 2023. Water-assisted growth of twisted 3R-stacked $MoSe_2$ spirals and its dramatically enhanced second harmonic generations. *Small* **19**, 2301828.
[173] Shearer M J, Samad L, Zhang Y, Zhao Y Z, Puretzky A, Eliceiri K W, Wright J C, Hamers R J and Jin S. 2017. Complex and noncentrosymmetric stacking of layered

metal dichalcogenide materials created by screw dislocations. *J. Am. Chem. Soc.* **139**, 3496–3504.
[174] Chang Y R, Higashitarumizu N, Kawamoto H, Chu F H, Lee C J, Nishimura T, Xiang R, Chang W H, Maruyama S and Nagashio K. 2021. Atomic-step-induced screw-dislocation-driven spiral growth of SnS. *Chem. Mater.* **33**, 186–194.
[175] Sun H B, Kong X, Park H, Liu F N, Lee Z and Ding F. 2022. Spiral growth of adlayer graphene. *Adv. Mater.* **34**, 2107587.
[176] Park H J, Tay R Y, Wang X, Zhao W, Kim J H, Ruoff R S, Ding F, Teo E H T and Lee Z. 2019. Double-spiral hexagonal boron nitride and shear strained coalescence boundary. *Nano Lett.* **19**, 4229–4236.
[177] Liu L L et al. 2019. Bottom-up growth of homogeneous Moiré superlattices in bismuth oxychloride spiral nanosheets. *Nat. Commun.* **10**, 4472.
[178] Wu J J et al. 2016. Spiral growth of $SnSe_2$ crystals by chemical vapor deposition. *Adv. Mater. Interfaces* **3**, 1600383.
[179] Zhuang A W, Li J J, Wang Y C, Wen X, Lin Y, Xiang B, Wang X P and Zeng J. 2014. Screw-dislocation-driven bidirectional spiral growth of Bi_2Se_3 nanoplates. *Angew. Chem., Int. Ed.* **53**, 6425–6429.
[180] Wang L et al. 2013. One-dimensional electrical contact to a two-dimensional material. *Science* **342**, 614–617.
[181] Watson A J, Lu W B, Guimarães M H D and Stöhr M. 2021. Transfer of large-scale two-dimensional semiconductors: challenges and developments. *2D Mater.* **8**, 032001.
[182] Li Y G, Kuang G Z, Jiao Z J, Yao L and Duan R H. 2022. Recent progress on the mechanical exfoliation of 2D transition metal dichalcogenides. *Mater. Res. Express* **9**, 122001.
[183] Dong W L, Dai Z H, Liu L Q and Zhang Z. 2024. Toward clean 2D materials and devices: recent progress in transfer and cleaning methods. *Adv. Mater.* **36**, 2303014.
[184] Li X S, Zhu Y W, Cai W W, Borysiak M, Han B Y, Chen D, Piner R D, Colombo L and Ruoff R S. 2009. Transfer of large-area graphene films for high-performance transparent conductive electrodes. *Nano Lett.* **9**, 4359–4363.
[185] Elías A L et al. 2013. Controlled synthesis and transfer of large-area WS_2 sheets: from single layer to few layers. *ACS Nano* **7**, 5235–5242.
[186] Yu H et al. 2017. Wafer-scale growth and transfer of highly-oriented monolayer MoS_2 continuous films. *ACS Nano* **11**, 12001–12007.
[187] Cao Y, Wang X H, Lin X Y, Yang W, Lv C, Lu Y, Zhang Y G and Zhao W S. 2020. Movable-type transfer and stacking of van der Waals heterostructures for spintronics. *IEEE Access* **8**, 70488–70495.
[188] Gurarslan A, Yu Y F, Su L Q, Yu Y L, Suarez F, Yao S S, Zhu Y, Ozturk M, Zhang Y and Cao L Y. 2014. Surface-energy-assisted perfect transfer of centimeter-scale monolayer and few-layer MoS_2 films onto arbitrary substrates. *ACS Nano* **8**, 11522–11528.
[189] Schneider G F, Calado V E, Zandbergen H, Vandersypen L M K and Dekker C. 2010. Wedging transfer of nanostructures. *Nano Lett.* **10**, 1912–1916.
[190] Zhang T Y, Fujisawa K, Granzier-Nakajima T, Zhang F, Lin Z, Kahn E, Perea-López N, Elías A L, Yeh Y T and Terrones M. 2019. Clean transfer of 2D transition metal dichalcogenides using cellulose acetate for atomic resolution characterizations. *ACS Appl. Nano Mater.* **2**, 5320–5328.
[191] Lu Z X, Sun L F, Xu G C, Zheng J Y, Zhang Q, Wang J Y and Jiao L Y. 2016. Universal transfer and stacking of chemical vapor deposition grown two-dimensional atomic layers with water-soluble polymer mediator. *ACS Nano* **10**, 5237–5242.
[192] Mondal A, Biswas C, Park S, Cha W, Kang S H, Yoon M, Choi S H, Kim K K and Lee Y H. 2024. Low Ohmic contact resistance and high on/off ratio in transition metal dichalcogenides field-effect transistors via residue-free transfer. *Nat. Nanotechnol.* **19**, 34–43.
[193] Magda G Z, Pető J, Dobrik G, Hwang C, Biró L P and Tapasztó L. 2015. Exfoliation of large-area transition metal chalcogenide single layers. *Sci. Rep.* **5**, 14714.
[194] Desai S B et al. 2016. Gold-mediated exfoliation of ultralarge optoelectronically-perfect monolayers. *Adv. Mater.* **28**, 4053–4058.
[195] Huang Y et al. 2020. Universal mechanical exfoliation of large-area 2D crystals. *Nat. Commun.* **11**, 2453.
[196] Fu Q et al. 2022. One-step exfoliation method for plasmonic activation of large-area 2D crystals. *Adv. Sci.* **9**, 2204247.
[197] Wu K et al. 2024. Gold-template-assisted mechanical exfoliation of large-area 2D layers enables efficient and precise construction of Moiré superlattices. *Adv. Mater.* **36**, 2313511.
[198] Grubišić-Čabo A, Michiardi M, Sanders C E, Bianchi M, Curcio D, Phuyal D, Berntsen M H, Guo Q D and Dendzik M. 2023. In situ exfoliation method of large-area 2D materials. *Adv. Sci.* **10**, 2301243.
[199] Jain A, Bharadwaj P, Heeg S, Parzefall M, Taniguchi T, Watanabe K and Novotny L. 2018. Minimizing residues and strain in 2D materials transferred from PDMS. *Nanotechnology* **29**, 265203.
[200] Purdie D G, Pugno N M, Taniguchi T, Watanabe K, Ferrari A C and Lombardo A. 2018. Cleaning interfaces in layered materials heterostructures. *Nat. Commun.* **9**, 5387.
[201] Hu J X et al. 2023. Controlled alignment of supermoiré lattice in double-aligned graphene heterostructures. *Nat. Commun.* **14**, 4142.
[202] Wang H and Qian X F. 2017. Giant optical second harmonic generation in two-dimensional multiferroics. *Nano Lett.* **17**, 5027–5034.
[203] Shen J C et al. 2025. Wafer-scale dry-transfer of single-crystalline transition metal dichalcogenides. *Adv. Mater.* **37**, 2504223.
[204] Kim K, Dasilva A, Huang S Q, Fallahazad B, Larentis S, Taniguchi T, Watanabe K, Leroy B J, Macdonald A H and Tutuc E. 2017. Tunable moiré bands and strong correlations in small-twist-angle bilayer graphene. *Proc. Natl Acad. Sci. USA* **114**, 3364–3369.
[205] Liao M Z et al. 2020. Precise control of the interlayer twist angle in large scale MoS_2 homostructures. *Nat. Commun.* **11**, 2153.
[206] Hsu W T, Zhao Z A, Li L J, Chen C H, Chiu M H, Chang P S, Chou Y C and Chang W H. 2014. Second harmonic generation from artificially stacked transition metal dichalcogenide twisted bilayers. *ACS Nano* **8**, 2951–2958.
[207] Hong H, Huang C, Ma C J, Qi J J, Shi X P, Liu C, Wu S W, Sun Z P, Wang E G and Liu K H. 2023. Twist phase matching in two-dimensional materials. *Phys. Rev. Lett.* **131**, 233801.
[208] Tang Y L et al. 2024. Quasi-phase-matching enabled by van der Waals stacking. *Nat. Commun.* **15**, 9979.
[209] Kim H, Choi Y, Lewandowski C, Thomson A, Zhang Y R, Polski R, Watanabe K, Taniguchi T, Alicea J and Nadj-Perge S. 2022. Evidence for unconventional superconductivity in twisted trilayer graphene. *Nature* **606**, 494–500.
[210] Park J M, Cao Y, Watanabe K, Taniguchi T and Jarillo-Herrero P. 2021. Tunable strongly coupled superconductivity in magic-angle twisted trilayer graphene. *Nature* **590**, 249–255.
[211] Anđelković M, Milovanović S P, Covaci L and Peeters F M. 2020. Double moiré with a twist: supermoiré in encapsulated graphene. *Nano Lett.* **20**, 979–988.
[212] Zhou W Q, Ding J, Hua J N, Zhang L, Watanabe K, Taniguchi T, Zhu W and Xu S G. 2024. Layer-polarized ferromagnetism in rhombohedral multilayer graphene. *Nat. Commun.* **15**, 2597.

[213] Kang K, Lee K H, Han Y M, Gao H, Xie S E, Muller D A and Park J. 2017. Layer-by-layer assembly of two-dimensional materials into wafer-scale heterostructures. *Nature* **550**, 229–233.

[214] Liao M Z et al. 2018. Twist angle-dependent conductivities across MoS_2/graphene heterojunctions. *Nat. Commun.* **9**, 4068.

[215] Liao M Z et al. 2022. UItra-low friction and edge-pinning effect in large-lattice-mismatch van der Waals heterostructures. *Nat. Mater.* **21**, 47–53.

[216] Kapfer M et al. 2023. Programming twist angle and strain profiles in 2D materials. *Science* **381**, 677–681.

[217] Schniepp H C, Kudin K N, Li J L, Prud'homme R K, Car R, Saville D A and Aksay I A. 2008. Bending properties of single functionalized graphene sheets probed by atomic force microscopy. *ACS Nano* **2**, 2577–2584.

[218] Yang Y P, Li J D, Yin J, Xu S G, Mullan C, Taniguchi T, Watanabe K, Geim A K, Novoselov K S and Mishchenko A. 2020. In situ manipulation of van der Waals heterostructures for twistronics. *Sci. Adv.* **6**, eabd3655.